# Power Module Packaging in Automotive Applications

by

Muhammed Rasit Atelge

A thesis
presented to the University of Waterloo
in fulfillment of the
thesis requirement for the degree of
Master of Applied Science
in
Mechanical Engineering

Waterloo, Ontario, Canada, 2016

# AUTHOR'S DECLARATION

I hereby declare that I am the sole author of this thesis. This is a true copy of the thesis, including any required final revisions, as accepted by my examiners.

I understand that my thesis may be made electronically available to the public.

# Abstract

In this study, nano silver paste was used as die attach material with the aim of increasing reliability of joints in power modules in automotive applications. Prior to joining, nano silver paste was spread on the interface between silver coated copper substrates and dummy chips by screen printing method. 5 groups of samples were produced using three different joining techniques based on different combinations of ultrasonic force and persistent pressure in air and vacuum atmospheres. The bonding quality of the interface region was evaluated by microstructural examination and quasi-static shear tests. On the other hand, electrical properties of sintered nano silver particles within the joints were characterized through resistivity measurements.

Sintered nano silver regions in all samples exhibited two types of porosity, namely, macro and micro porosity. Macro pores formed during the evaporation and removal of organics present in the starting paste, while micro pores were left in the structure because of insufficient sintering of silver nano powders. Although the sintered silver interface in samples produced using 5 MPa persistent pressure in air displayed a minimum amount of porosity, pores as large as 5 μm in diameter were observed in joints produced in air by a preload of 0.01 MPa with or without ultrasonic force. In addition, vacuum sintering yielded relatively porous interfaces compared to samples manufactured in air even though the same compaction pressure was applied during sintering. Accordingly, in the samples produced either in air by the application of low preloads of 0.01 MPa or in vacuum at 5MPa, additional microcracks were formed, particularly in the interface region between silver coating and sintered nano silver particles.

Stress-strain curves of the joints exhibited linear elastic, small strain hardening and fracture regions similar to wrought alloys. The strengths of the joints increased proportionally to the degree of sintering as expected. The shear strength reached to ~32 MPa in samples sintered in air at 5 MPa constant pressure, whereas shear strength decreased to ~4 MPa in highly porous joints produced by ultrasonic force and preloading with 0.01 MPa. All samples revealed shear-type dimples in the direction of mechanical testing indicating ductile behavior of joints.

The electrical resistivity of the sintered nano silver layer showed the same trend as the mechanical properties. The weakest or most porous joint had the highest electrical resistivity of approximately 125.5 μΩ-cm). On the other hand, the least porous silver joint, manufactured at 5 MPa constant pressure in air

exhibited the lowest electrical resistivity (7.8 μΩ-cm); however, it was five times higher than that of bulk silver.

The results have presented that the nano silver paste is the most promising die attach material to replace conventional solder and conductive epoxies.

Keywords: Die attach material, nano silver paste, sintering, shear strength, electrical resistivity

# Acknowledgements

I would like to offer my sincere thanks to Dr. Mustafa YAVUZ and Dr. Eihab ABDEL-RAHMAN for their support and supervision.

Special thanks to Dr. Ziya ESEN for his enormous efforts and helps throughout my research project.

I would like to thank all of our group members, especially, Dr. Mahmoud KHATER, Dr. Sangtak PARK and Turker DAGDELEN for their management and help.

I would like to acknowledge and thank Takatoshi NISHIMURA and his company (Nihon Superior CO., LTD) for their support of my study.

I greatly appreciate the Turkish Republic Ministry of National Education for their continuous financial support throughout my master's degree education.

Lastly, I am thankful to my lovely family.

# Dedication

To my lovely family

# Table of Contents

# List of Figures

# List of Tables

# Chapter 1
# Introduction

## 1.1 Background

The widespread use of fossil fuels is responsible for the long-term environmental risk of climatic changes. The key contributor to global warming is the emission of carbon dioxide ($CO_2$) that comes from many combustion sources. According to the Inventory of the United States Greenhouse Gas (GHG) Emissions and Sinks 1990–2013 report published by the United States Environmental Protection Agency (EPA), GHG emissions from transportation represented 27% of the total amount of US GHG emissions from end-use fossil fuel combustion in 2013. Passenger cars (42.7%), light-duty trucks (17%) and medium/heavy-duty vehicles (22.8%) were culpable for 82.5% of the $CO_2$ emitted from all transportation sources [1]. The maximum allowable levels of tailpipe emissions from diesel engines have also becoming stricter under current legislation. In 1999, the European Union (EU) adopted Directive 1999/96/EC, which presented Euro III emission standards in 2000 and Euro IV/V standards in 2005/2008. In European countries, which have integrated the Euro V emission standard for vehicles, the Euro VI emission standard has been carried out since 2014. The Euro VI emission standard needs additional improvement step by step to reduce tailpipe emissions, particularly $NO_x$, for heavy-duty and non-road engines [2]. Attempts to reduce harmful emissions of all types led to the conclusion that the problem may be solved by the production of electric vehicles, which use electric motors and require a high volume of high-temperature power electronics.

Power electronics convert electric power from one type to another using electronic devices, and the power level may vary from mW to GW such as in small batteries and power plant applications, respectively [3].

Devices in power electronics can be grouped into four categories according to the type of their input and output power [3]:

• AC/DC, a rectifier is an electrical device that converts alternating current (AC), which periodically reverses direction, to direct current (DC), which flows in only one direction. For example, standard outlet voltage is converted to 5V DC for smartphone charging.

• DC/AC, a power inverter changes direct current (DC) to alternating current (AC). For example, the DC of a battery pack of an electric vehicle (EV) is converted to the AC of the desired amplitude and frequency for driving an electric motor.

• DC/DC, a DC-to-DC converter switches a source of direct current (DC) from one voltage level to another.

• AC/AC, a solid-state AC-AC converter switches from an AC waveform to another AC waveform, where the output voltage and frequency can be set.

In electric vehicles (EVs), a battery pack is utilized for energy storage and electric motors are used to transfer power to the wheels. Therefore, different parts of the system in automobiles require various types of converters. Firstly, to convert the DC power into AC power, an inverter is needed. It is possible to switch the speed and power of the electric motor with the inverter. Most of the electric systems in conventional internal combustion vehicles operate at 12 V or 24 V. In EVs, the voltage of the battery pack is generally greater than the voltage of the electric motors used to power the wheels. Therefore, DC/DC conversion is used to regulate the voltage levels to meet predetermined systems requests [3]–[5]. As electrical energy becomes more dominant in electrical vehicles such as hybrid-electric vehicles (HEVs), plug-in hybrid electric vehicles (PHEVs), fuel cell electric vehicles (FCEVs), and pure electric vehicles (EVs), the study of power electronics systems under harsh environmental conditions related to automotive applications is essential [6].

In power electronics, a power semiconductor device is a semiconductor device used as a switch or rectifier. Semiconductor devices are used to alter the voltage and current [7] and they are classified as uncontrollable and controllable power semiconductors. Power diodes, and thyristors and transistors are the examples of uncontrollable and controllable semiconductors, respectively. Metal-Oxide-Semiconductor Field-Effect Transistors (MOSFETs), Bipolar Junction Transistors (BJTs) and, Insulated Gate Bipolar Transistors (IGBTs) give complete control of "on" and "off" states [6].

Recently, IGBTs, as shown in Figure 1.1, have been largely used for power applications because of their working range of 300 V to over 6.5 kV [8] and high switching speed, on-state voltage drop and ruggedness [6]. Although precise control of power is possible with devices such as IGBTs, high operating temperatures limit the performance and reliability of such devices. Therefore, redesign of the device materials is needed especially in their interconnections capable of withstanding high temperatures without degrading electrical properties [9].

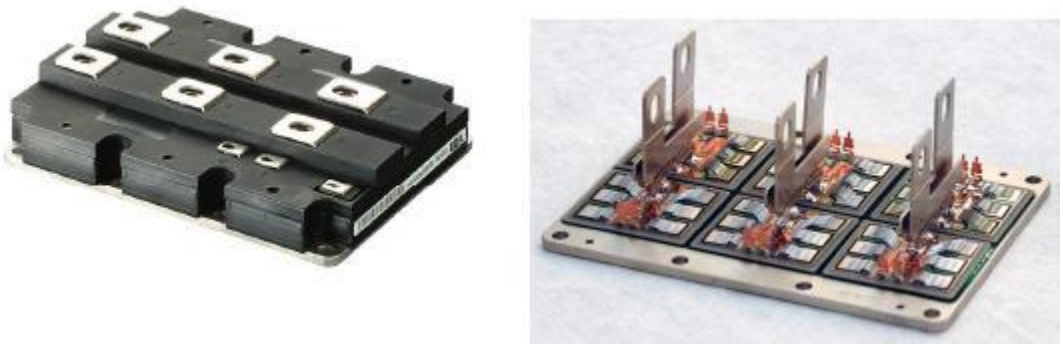

Figure 1.1 1200Amp., 3300V IGBT Module [10].

## 1.2 Motivation

In a power electronics device, the power losses are created within the "on"- "off" state of the device. As the level of losses change between various operating conditions, the power device temperature will also change with time. The thermal energy, which is created during the "on"- "off" state, flows along the thermal path. Conventional IGBT modules, Figure 1.2, consist of a Si chip, direct copper bonded (DBC) substrate, copper or AlSiC heat sink and solder interconnections materials. Generated heat in such a module flows from chip to heat sink and dissipates into the air.

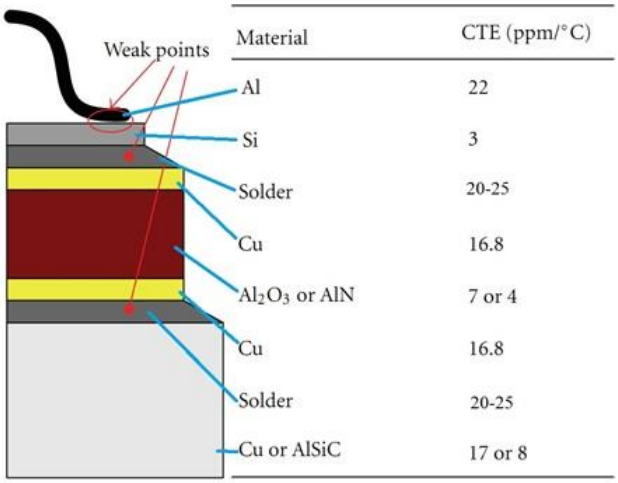


Figure 1.2 Traditional IGBT Cross-Section showing various components with their CTEs [11].

Differences between the coefficients of thermal expansion (CTE) of material layers defined in IGBTs induce stress during thermal flow. In addition, the stress is created not only on different material layers, but also within the same type of material due to temperature differences along the thermal path [12].

However, most of the thermal stress induced failure occurs within the interlayers which are used for connection of different material layers. Commonly used interconnection materials or die attach materials are conductive adhesives, and tin based and lead free solder alloys in power electronics.

The maximum processing temperature of conductive adhesives is lower than 200 $^{O}$C while it is below 250 $^{0}$C for tin based alloys [13]. The low melting point of these die attach materials is one of the main problems encountered during their usage at high temperatures above 200$^{o}$C. When using them at high temperature, their intermetallic phases are high and as a result, their reliability may decrease. Additionally, using encapsulated materials increases the operating temperature, which reveals the mismatch of CTE. Thus, their reliability has an undesirable effect [14]. Due to the different elongation of layers, the repetitive stress changes cause fatigue of interconnection materials in IGBT modules. That creates crack initiation, crack elongation and failure.

The interconnection material is one of the most problematic components in the IGBT modules. In this thesis, we focused on nano silver paste as a new generation interconnection material. The nano silver paste was investigated using fabrication processes in air and vacuum. To develop this new fabrication method, ultra-sonic force was used. Mechanical properties of nano silver paste were compared with the literature. Additionally, samples, which were fabricated with different joining techniques in air and vacuum were compared to each other. Electrical resistivity of the sintered nano silver layer was measured. Microstructure study was performed for each fabrication process.

# Chapter 2
# Literature Review

## 2.1 Literature Review

### 2.1.1 IGBT for Automotive Applications and Trends

Electric drive vehicles such as hybrid-electric vehicles (HEV), plug-in hybrid electric vehicles (PHEV), fuel cell electric vehicles (FCEV), and pure electric vehicles (EV) need power electronics for conversion of electric energy from the battery to the desired form. This energy can be used directly to power the wheels or to assist with the traditional combination engine system. In the past decade, increased popularity of HEVs and EVs has generated great attention related to power electronics and power semiconductors manufacturing technology. In electric drive systems of vehicles, power modules constitute approximately 40 % of the price of inverters and converters. In the next decade, the market of power modules for the automotive industry is expected to grow from $2 billion to $5 billion [15].

In EVs, power modules include various power semiconductor switches such as DC to DC converters, DC to AC inverters and insulated gate bipolar transistors (IGBTs). To meet an urgent request for automotive power modules, reliability standards are needed especially for those operating under harsh working environments including high operating temperature, high ambient temperature and mechanical vibration. Improvement of materials used in packaging of the power modules is one of the key aspects in increasing their reliability [15].

In the past few decades, chip technology has been developed to improve power modules. The market requests were satisfied with conventional design and joining technology. As a consequence, the cross sectional structure of power modules has had very limited improvements [16]. Nonetheless, these requirements have been changed recently due to:

- The performance of power electronics mainly depends on packaging technology,
- The automotive industry requires cost effective production and compactness,
- New chip technologies are needed as wide band gap materials such as silicon carbide (SiC) or gallium nitride (GaN) are utilized as chip materials.

Moreover, new packaging technologies and materials capable of withstanding junction temperatures above 200 $^{0}$C are desired in addition to the aforementioned requirements [16].

The cross-section of the conventional power module packages shown in Figure 2.1 has developed over a few decades. Several improvements have been accomplished step by step to increase electrical performance and reliability, and to decrease the die size of such packages over the last 30 years. The reliability of packages is crucial, particularly in EVs, as 14 years average lifetime is expected for such automobiles [17]. During usage of an EV, the temperature fluctuations occurring in power electronic devices or power modules induces thermal stresses due to materials having different coefficients of thermal expansion (CTE) across the module, Figure 2.1, [16].

Currently, the traditional packaging techniques have not met some service requirements such as high operating temperature. Therefore, research on new interconnection materials and new joining techniques has gained attention.

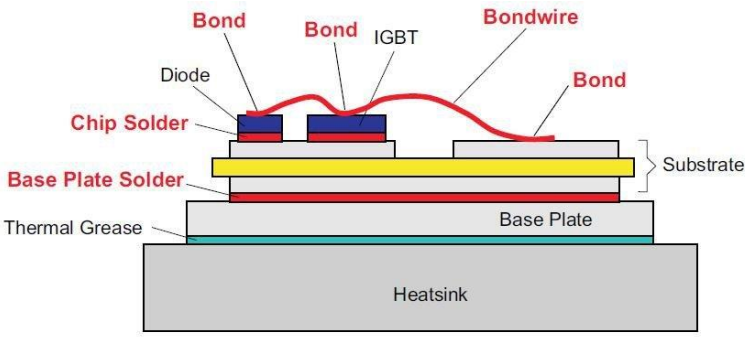


Figure 2.1 Cross-section of a conventional IGBT module [18]

### 2.1.2 Die Attach Materials

In microelectronic packaging, interconnection materials provide physical protection, mechanical support, electrical connection, and heat dissipation for semiconductor devices to fulfill a function in a specific condition [19]. Die attach material, which connects the die to the substrate and the substrate to the rest of the system, plays a key role to ensure that the whole system works consistently. Tin-based solder alloys such as leaded (63%Sn-37%Pb) and lead-free solder alloys (96.5%Sn-3%Ag-0.5%Cu), Table 2.1, and conductive adhesives are commonly accepted die attach materials. Since their fabrication parameters are below 300 $^{0}$C and they are easily used, they are preferred as die attach materials [20]. Although rich lead solder alloys show high reliability in harsh working conditions, their use in microelectronic packaging is restricted according to hazardous substances directive 2002/95/EC [21]. However, the tin based solder

alloys and conductive adhesives suffer from low melting and/or dissociation temperatures when used in high temperature applications (>200 $^0$C) such as automotive, gas and down-oil.

Table 2.1 Commonly used solder materials properties [22], [23].

| **Properties** | **Unit** | **Eutectic Solder (63Sn-37Pb)** | **96.5Sn-3.0Ag-0.5Cu Lead-Free Solder** |
|---|---|---|---|
| **Density** | g/cm$^3$ | 8.4 | 7.4 |
| **Hardness (Vickers/Brinell)** | HV/HB | 14 HV | 15 HB |
| **Tensile Strength (Ultimate)** | MPa | 52 | 49.6 |
| **Modulus of Elasticity** | GPa | 32 | 51 |
| **Poisson's Ratio** | - | 0.38 | 0.36 |
| **Shear Modulus** | GPa | 12 | |
| **Melting Point** | $^o$C | 183 | 220 |
| **Thermal Conductivity** | W/(mK) | 50.9 | 58 |
| **CTE at room temperature** | μm /m$^o$C | 24.7 | 21.6 |
| **Electrical Resistivity** | μΩ-cm | 14.5 | 13.2 |
| **Homologous Temperature According To 200 $^o$C Operating Temperature** | - | >100% | 96% |

The homologous temperature, the ratio of operation and melting temperatures in K scale, is important in terms of reliability and a material can be considered as stable when its homologous temperature percentage is below 40%. If the homologous temperature is between 40-60%, the material is operating in the creep region while a homologous temperature percentage above 60% is considered to be an unstable range for the material. Operating temperatures of approximately 200 $^0$C correspond to the unstable region for solder materials which prevents their safe usage as a die attach material [12]. Other die attach materials such as conductive adhesives containing a high ratio of polymeric materials have lower electrical and thermal conductivities, and also lower melting points than solder materials. Therefore, in power modules, new die attach materials are needed with the following properties[14], [24], [25]:

- Low coefficient of thermal expansion (CTE) between layers,
- High electrical conductivity,
- High thermal conductivity,
- Excellent mechanical properties,
- Excellent fatigue resistance,
- Good corrosion resistance,
- Good wettability and adhesion to the die and the substrate.

In a vehicle's engine, the operating temperature may increase up to 1000$^o$C. To achieve more accurate control of the valve on-off timing, sensing of camshaft position and engine pressure is a way to alleviate the emission problem. Therefore, using sensors in automobiles has significantly increased the preciseness of measurements [26]. Currently, advanced vehicles have about a hundred sensors, measuring such things as engine speed, camshaft position, engine condition monitoring, and brake system [14]. Many of the automotive electronics components withstand high operating temperature such as brake system sensors (up to 300 $^0$C), and combustion sensors (up to 1000 $^0$C). To manage the electric current flow from battery pack to the electric motor, a power module is necessary equipment for this vehicle. [9]. The weakest point of all of these components is die attachment materials.

One of the requirements of power electronics is the high operating temperature. The definition of high temperature, which can generally differ according to electronic applications, is the highest ambient temperature or a typical standard operating temperature. As high temperature, it may be chosen as ambient temperature if the junction temperature is lower than ambient. However, with high power

dissipation at some specific points and densely packaging design, self-heating should take into account because the junction temperature becomes the dominant heat source of system such as power modules [27]. Some applications, for example automotive, aircraft, and space exploration, need to withstand operating temperatures above $200^0$C for die attach materials [14].

Power modules have been recently improved due to innovations in materials, interconnections, and processing techniques [15]. In the automotive industry, the electrical performance of the power modules is mostly effected by the packaging technology of these devices [28]. The demand of the power modules is electrical, thermal, and reliability performance with compact design. There are some packaging problems for IGBT modules and one of the most important is interconnection [29].

As mentioned above, high power modules have been widely used under harsh operating conditions in the automotive industry. Figure 2.2 shows operating temperatures of different automotive systems [9]. The entire power module can fail completely because of high heat dissipation, which exceeds the acceptable levels of the devices. Furthermore, higher power density creates a very high junction temperature in the chip. It affects the device performance, plus it causes reduction of semiconductor life [30]. In IGBTs, static thermal flux is between 100 W/cm$^2$ and 300 W/cm$^2$ when used in automotive applications [31]. The ability to attach a chip with a large area is one of the most significant parts in power modules. Improving the lifetime of the device is possible when a good thermal conductive material as a die attach material is used.

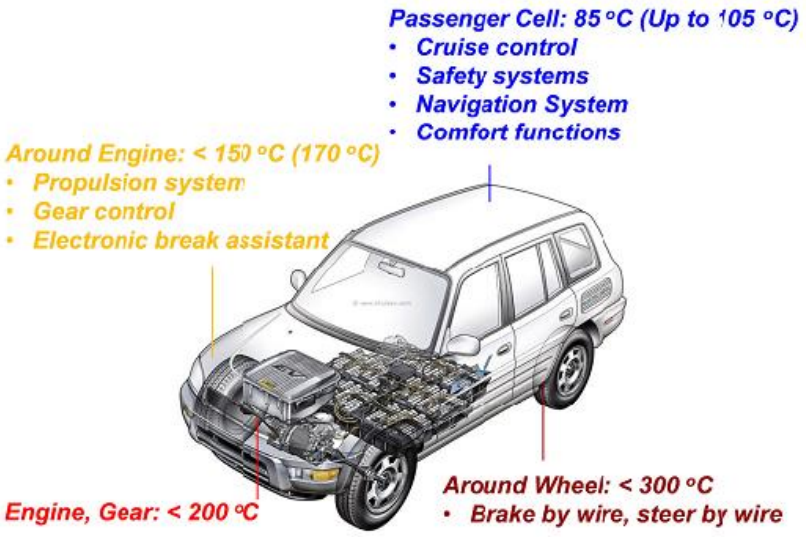


Figure 2.2 Automotive operating temperatures [5, 33].

Some lead free solders such as AuSi, AuGe, and AuSn exhibit good reliability even in harsh environments. However, their high prices block their usage in power modules [30].

Currently, nano silver powder containing paste is reported as a superior die attach material in terms of electrical and thermal conductivity and mechanical properties [12], [25], [32]–[35]. The sintered silver paste has not only higher thermal and electrical conductivity but also higher tensile strength compared to commonly used solder alloys, Table 2.2. However, the most significant advantage of this paste is its relatively higher melting point which makes the connections reliable at higher temperatures. Accordingly, it compensates for all the weak points of packaging technology encountered due to the solder and conductive adhesive die attach materials.

Table 2.2 Comparison of sintered nano silver and traditional solder materials (Compiled from [12], [22], [23], [25], [32]–[35])

| **Properties** | **Unit** | **Sintered Nano Silver**[1] | **Eutectic Solder (63Sn-37Pb)** | **96.5Sn-3.0Ag-0.5Cu Lead-Free Solder** |
|---|---|---|---|---|
| **Density** | $g/cm^3$ | 3.5 | 8.4 | 7.4 |
| **Hardness (Vickers/Brinell)** | HV/HB | - | 14 HV | 15 HB |
| **Tensile Strength (Ultimate)** | MPa | 55 | 52 | 49.6 |
| **Modulus of Elasticity** | GPa | 10-30 | 32 | 51 |
| **Poisson's Ratio** | - | 0.37 | 0.38 | 0.36 |
| **Shear Modulus** | GPa | 27.8 | 12 | |
| **Melting Point** | $^oC$ | 961 | 183 | 220 |
| **Thermal Conductivity** | W/(mK) | 240 | 50.9 | 58 |
| **CTE at room temperature** | $\mu m/m^oC$ | 19.6 | 24.7 | 21.6 |
| **Electrical Resistivity** | $\mu\Omega$-cm | 2.5-5 | 14.5 | 13.2 |
| **Homologous Temperature percentage According to operating Temperature of 200 $^oC$** | - | 38% | >100% | 96% |

[1] Sintered nano silver properties depend on its fabrication parameters.

### 2.1.3 Silver Joints

Silver, like gold, is one of the precious metals. Silver is a 4d transition element, atomic number 47, atomic weight 107.87, and electron configuration [Kr]4d105s1. In the periodic table, silver is placed in period 5, group 11 (or IB). It is a soft and ductile material with face-centered cubic structure and melting point of 961.93° C, Table 2.3. It possesses the highest electrical and thermal conductivity of any element. Silver is generally utilized in electrical contacts and thermal conductors in the microelectronics industry as well as in photography, jewellery, silverware, coins, and medals [36].

Table 2.3 Properties of bulk silver [35], [36].

| **Properties** | Unit | Silver (Ag) |
|---|---|---|
| **Density** | $g/cm^3$ | 10.491 |
| **Hardness (Vickers)** | HV | 25 |
| **Tensile Strength (Ultimate)** | MPa | 140 |
| **Modulus of Elasticity** | GPa | 76 |
| **Poisson's Ratio** | - | 0.37 |
| **Shear Modulus** | GPa | 27.8 |
| **Melting Point** | $^oC$ | 961.93 |
| **Thermal Conductivity** | W/(mK) | 419 |
| **CTE at room temperature** | $\mu m/m^oC$ | 19.6 |
| **Electrical Resistivity** | $\mu\Omega$-cm | 1.55 |

In 1989, the service requirements of power modules could not be met by traditional joining techniques to bond substrates and chips together. Sintered silver joining has been developed by Schwarzbauer et al. [37] as a novel method. It is also known as a low temperature joining technique (LTJT), Figure 2.3. Diffusion bonding is the underlying reason for low temperature solid state joining. In the study of

Schwarzbauer et al.[37], the surface of substrate and chip were coated with a thin layer of Au or Ag. Finally, silver flakes were placed between these two layers as interconnection material and sintered at 240$^{o}$C with 40 MPa pressure. Recently, low temperature joining technique has been studied with different kinds of metallic nanoparticle pastes of Ag [12], [25], [32]–[35], Cu [38], Au [39], Ag-Al alloy [40], and, Ag-Cu alloy [41]. In Ag joining processes, nano silver paste containing silver powder (micron and/or nano size), organic solvent and binder is recently used as a die attach material. Since silver paste has been introduced as a superior lead free die attach material by the European power electronic companies, LTJT using silver paste has gained great attention from academia and industry players.

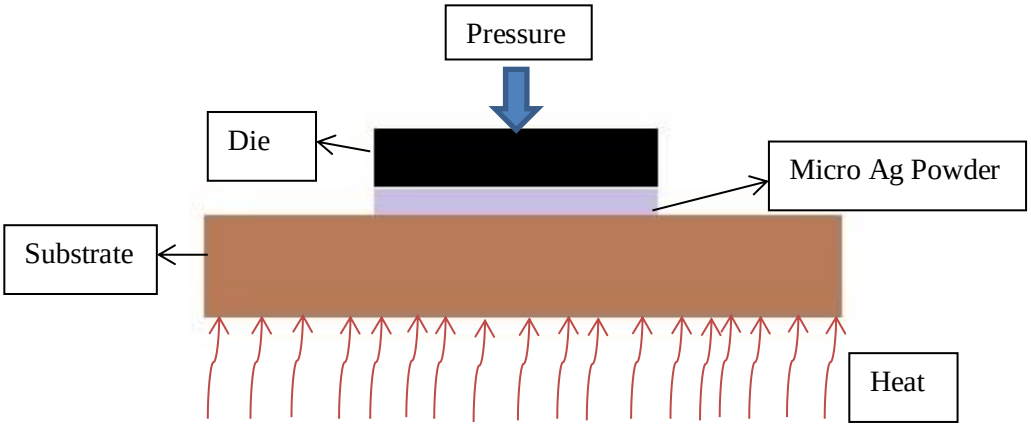


Figure 2.3 Low Temperature Joining Technique using silver powders

### 2.1.4 Joining Processes Using Nano Silver Paste

#### 2.1.4.1 General

Most silver joining is formed by utilizing powder metallurgy. Powder metallurgy is a process, which includes the fabrication, characterization and change of metal powders into valuable engineering materials. The process includes the use of fundamental laws of heat, work, and deformation of the powder. The shape, properties and structure of the powder are changed as a final material. Powder metallurgy starts with the preparatory production of a shaped article from finely divided powders either by hand or by utilizing mechanical compaction. The next step is a sintering process in a furnace to increase the strength of the component without losing the initial shape during molding [42].

When the powders are heated up to approximately half of their absolute melting temperature, the powder particles are bonded to each other. This phenomena is called sintering [43]. The sintering process is performed with or without pressure either in a liquid state or a solid state as in most of the silver-joints.

Starting powders with various shapes, i.e. flake, angular, spherical, may be elemental or pre-alloyed powders. In solid state sintering, various stages and mass transport mechanisms have been utilized as shown in Figure 2.4.

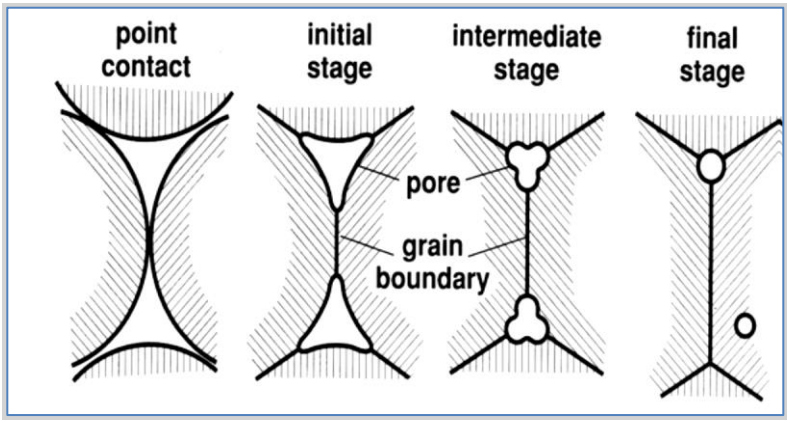


Figure 2.4 Solid State Sintering Stages [44]

In the sintering process, to minimize the surface energy, the system attempts to decrease the surface area. Consequently, the particle is bonded to adjacent particles and the bonding turns into the neck. In the next stage, the pore structures become smooth and approximately cylindrical shaped. Decrease in surface area decreases the time required for sintering. In the final stage of solid state sintering, structural pores have almost vanished and the remaining pores are separated from each other. Based on the time and temperature of sintering, various mass transport mechanisms, illustrated in Figure 2.5, become operative which induces neck formation and densification in solid state sintering [42].

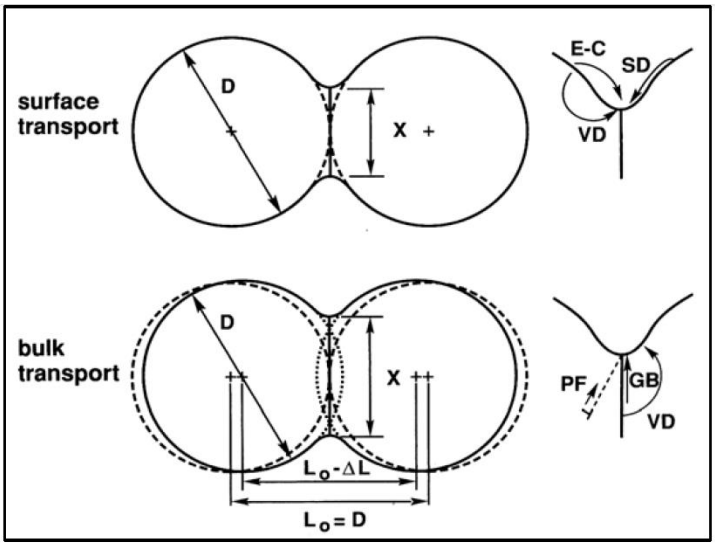


Figure 2.5 Two classes of mass transport mechanisms encountered during sintering; Evaporation-Condensation (E-C), Surface Diffusion (SD), Volume Diffusion (VD), Plastic Flow (PF), Grain Boundary Diffusion (GB) [44]

As the particle size of the powders decrease, sintering and densification becomes easier due to increased surface area. Although most of the powder metallurgical processes make use of micro sized powders, recently the use of nano size powder has gained great attention. When particle size is reduced to nano scale dimensions, 1-100 nanometers, materials break the barrier of quantization of energy for the electrons in solids and their properties dramatically change and even exhibit new properties [45].

Sintered silver joint was firstly developed in the early 1990s using micro size silver flakes [37]. The method was basically a sintering technique in which the variables were chosen as temperature and pressure. At 250 $^0$C, connection of parts was produced by compaction of flake shaped silver powders under the pressure of 9-40 MPa. In the middle of the 2000s, discovery of nano materials took this technique to the next level. The temperature of the process has stayed at the same level; however, the pressure in the "pressure assisted sintering" has been significantly decreased around 1-5 MPa when the nano particles of silver were used. In such processes, silver nano particles are supplied in the form of silver-paste containing a kind of binder and dispersant solution which acts as a binder and carries nano particles and controls the viscosity of the paste. The sintering mechanism of those silver pastes is also affected by the size of the silver particles inside the paste and the paste chemical formulation. In nano scale, the driving force for diffusion bonding of silver atoms is increased due to increased surface energy. A 26 nm silver nano particle surface area was reported 23 $m^2$/g [46]. In sintering processes including nano

silver powders, neck size quickly grows until the neck size reaches 50% of the nano particle size before the sintering rate slows down [47].

Power electronics and other applications which use silver-paste as a die attach material look for sintering processes at pressures and temperatures as low as possible within the shortest time possible. The use of nano silver powders partly meets the needs of sintering requirements in die attachments. However, researchers still investigate techniques which will reduce the sintering temperature, pressure and time in the joining process while avoiding degradation of strength of sintered silver joints. In addition, types of organics and their removal is another issue for silver-paste containing sintering processes. Organic solvents in silver pastes evaporate at around 100$^{o}$C as a result of an endothermic process which can be detected with a differential scanning calorimetric and thermo gravimetric analysis to observe thermal events and their effects on sintered silver joining [48].

Most of the studies use cyclohexanol, terpineol, ethylene glycol ether, or cyclohexanol–methanol mixture as organic solvents in silver-pastes to mix micron sized silver flakes [48]. Joining processes which make use of these pastes are achieved under 9 – 40 MPa pressure at 180 – 250 $^{0}$C [37]. On the other hand, for nano sized silver particles, the paste consists of nano size silver particles which are less than 100 nm, solvents, dispersants and binder. Siow [50] gave a summary of solvents, dispersants and binders previously used by many researchers. Solvents were reported to be isobornyl cyclohexanol (IBCH), texanol, terpineol, butyl carbitol, toluene, xylene, ethanol, or phenol while ethyl cellulose, polyvinyl alcohol, polyvinyl butyral (PVB), or waxes were used as binders. Menhaden fish oils, poly(diallydimethyl ammonium chloride) (PDDA), polyacrylic acid (PAA), polystyrene sulfonate (PSS), triethylene glycol, methyloctylamine, dodecylamine, hexadecylamine, myristyl alcohol, 1-dodecanol, 1-decanol stearic acid, oleic acid, palmitic acid, dodecanethiol are some examples of dispersants used in addition to solvents and binders. Although the pressure of the nano silver process decreases to 1 – 10 MPa, the temperature of the process is higher, 200 – 300 $^{o}$C, compared to micron size silver containing pastes. It is also possible to use silver paste for connection of joints without added pressure. In this case, organic components of the paste decrease from 15 % to 4% while the quantity of nano silver particles increases above 90% by weight. Usually during the sintering process, pressure is not needed because of the reactive nature of the paste. However, the die size determines the application of the pressure during sintering. When the die size is smaller, diffusion of oxygen and outgassing of solvent from the small sintering area becomes easier. Therefore, the shear strength of the pressureless sintered interface layer is as strong as those sintered under pressure assisted conditions. [48].

### 2.1.4.2 Conventional Joining Methods using Sintered Silver Paste

The performance of joining produced by using silver-paste is strongly dependent on the application procedure of the paste on the surface, removal of organics and sintering variables used in the process. For mounting of nano silver paste on substrate, the screen-printing method is widely used. For the purpose of evaporation of solvent and elimination of subsequent solvent related residual porosity, the paste containing structure is preheated to approximately 50–100 $^{o}$C prior to sintering. After preheating treatment, dies are mounted onto the paste containing substrate. Then, the sandwich configuration containing die, nano silver paste and substrate, is heated to the predetermined sintering temperature. When the sintering temperature is reached, pressure is applied and all the sintering process is carried out under pressure assisted condition. The screen printing method of silver-paste and the commonly used temperature profile in the process are shown in Figure 2.7 screen printing method and Figure 2.7 sintering cycle used for silver-paste containing joints.

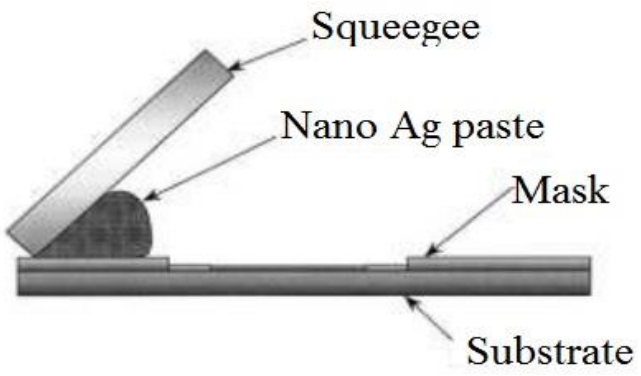


Figure 2.6 Screen printing method

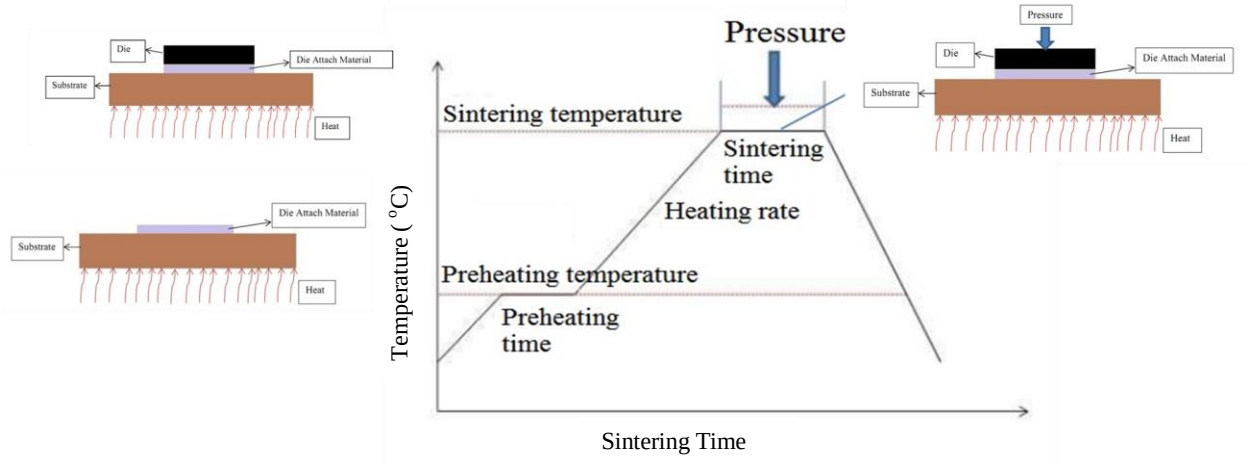


Figure 2.7 Sintering cycle used for silver-paste containing joints

#### 2.1.4.2.1 Processing Parameters in Nano Silver-paste Containing Joints

Recently, nano silver paste has garnered great attention because of its superior success in die attachments. To bond semiconductor and substrate with silver-paste, several processing parameters should be considered to obtain strong bonds between die and the substrate. The shear strength is a primary evaluation tool to investigate the performance of nano silver joining. Pressure, sintering temperature, holding time, heating rate, substrate and chip metallization, and particle sizes have had an impact on bonding quality during fabrication. Appendix A gives a summary of studies carried out at various processing conditions using different silver based pastes and elementary silver powders. Commonly studied variables are the types of die attach materials and their sizes, coating of substrates and chips, sintering temperature, pressure and time, heating rate, test methods, and the shear strength of joining.

##### 2.1.4.2.1.1 Compaction Pressure

During the sintering process, applied external pressure helps the sintering as it increases the available contact area for diffusion of atoms thereby, increasing the shear strength of silver-joints. Figure 2.8 displays the effect of applied pressure during sintering on the shear strengths of joints in studies containing various die and substrate materials [49] (data compiled from [34], [50]–[53]). Increasing applied pressure improves bonding shear strength as expected since it yields better contact between nano silver particles and the substrate. Accordingly, the neck area between powder particles grows faster, and a high density nano silver sintered joining area with a less porous structure is obtained. Outgassing of

organic components, which burn out during sintering, leaves more joining area when external pressure is applied so that pressure assisted sintering has a higher density and shear strength.

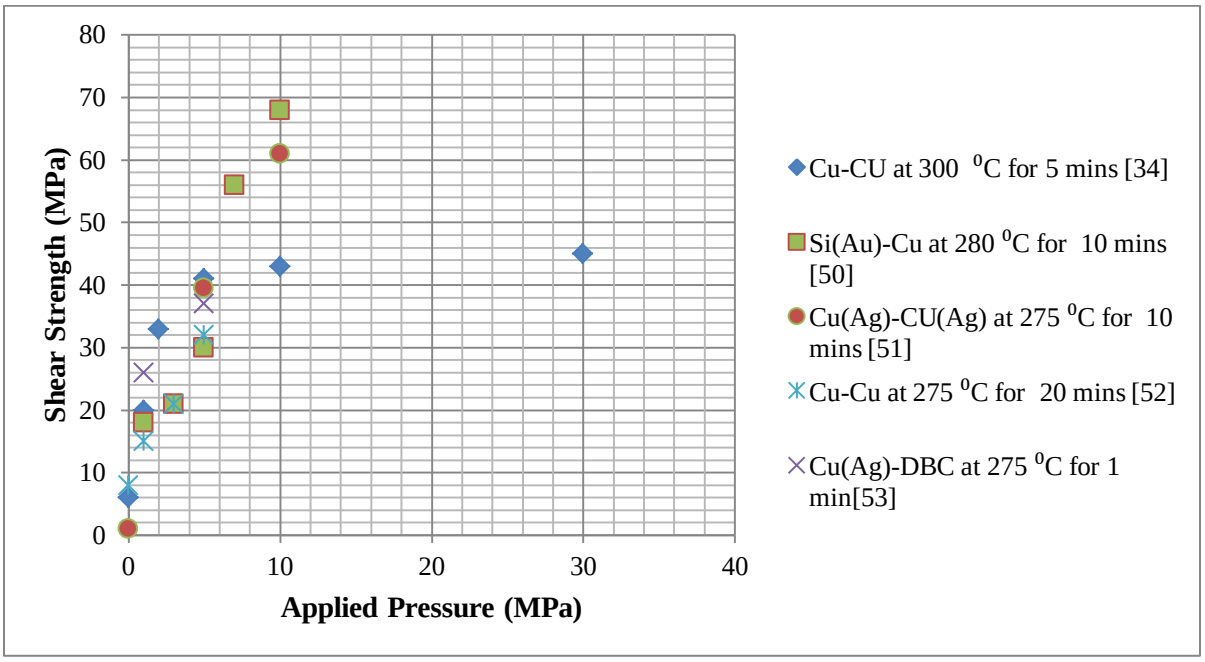


Figure 2.8 Pressure effect on shear strength of silver-containing joints[49]

### 2.1.4.2.1.2 Sintering Temperature and Time

Sintering temperature has a strong impact on bonding quality due to exponential dependence of diffusivity of atoms on temperature. Increasing sintering temperature generates an intense joining area by the mass transport of atoms via surface and/or bulk diffusion according to temperature used. To improve nano silver paste stability, large amounts of various organic materials are added. Therefore, burning of those organics also has an influence on sintering temperature and time, and resultant mechanical properties. Accordingly, burning and complete removal of organics is crucial so as to allow diffusion of silver atoms within nano silver-particles. Usually a higher sintering temperature provides higher and complete evaporation thereby increasing the rate of sintering. As presented in Figure 2.9 [49], higher temperatures increase the resultant shear strength because of enhanced sintering which leaves less residual porosity in the structure (data compiled from [35], [53]–[56])

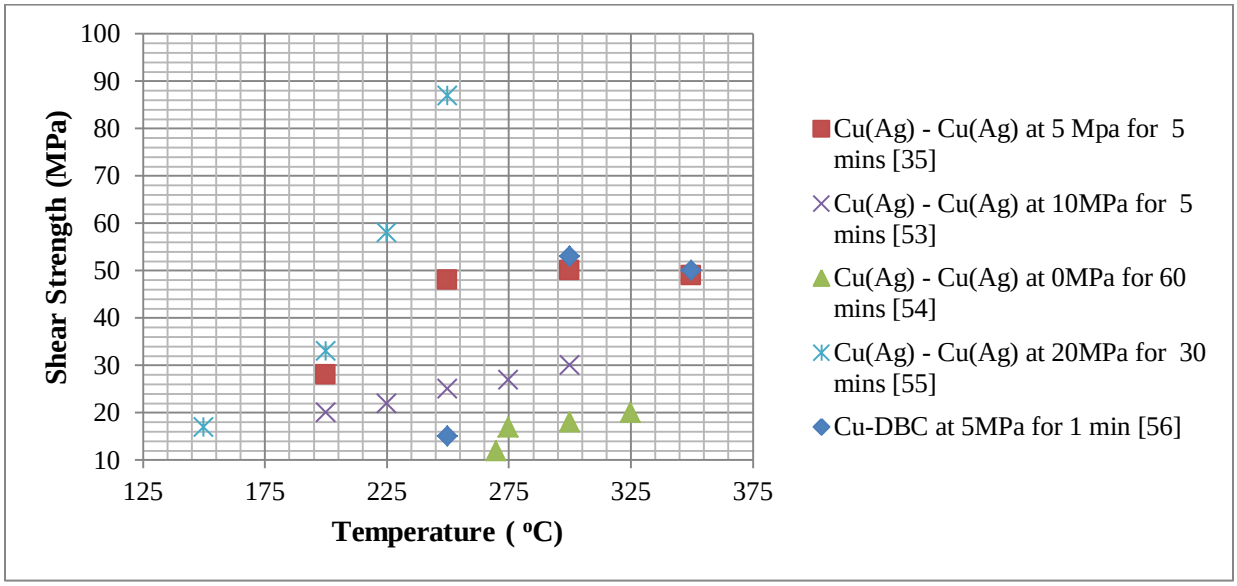


Figure 2.9 Relationship between shear strength of nano silver bonding and sintering temperature [49].

During sintering, longer sintering time increases neck size between nano particles and it helps depletion of organic materials inside the paste. As a result, shear strength is improved with longer sintering time and better adhesion is observed as shown in Figure 2.10 [49] (data compiled from [33], [53], [54] ). However, the effect of sintering time is not as significant as sintering temperature since diffusion distance, x, changes by the square root of time ($x=\sim 2\sqrt{Dt}$, where D is diffusivity of atom interest and t is the time).

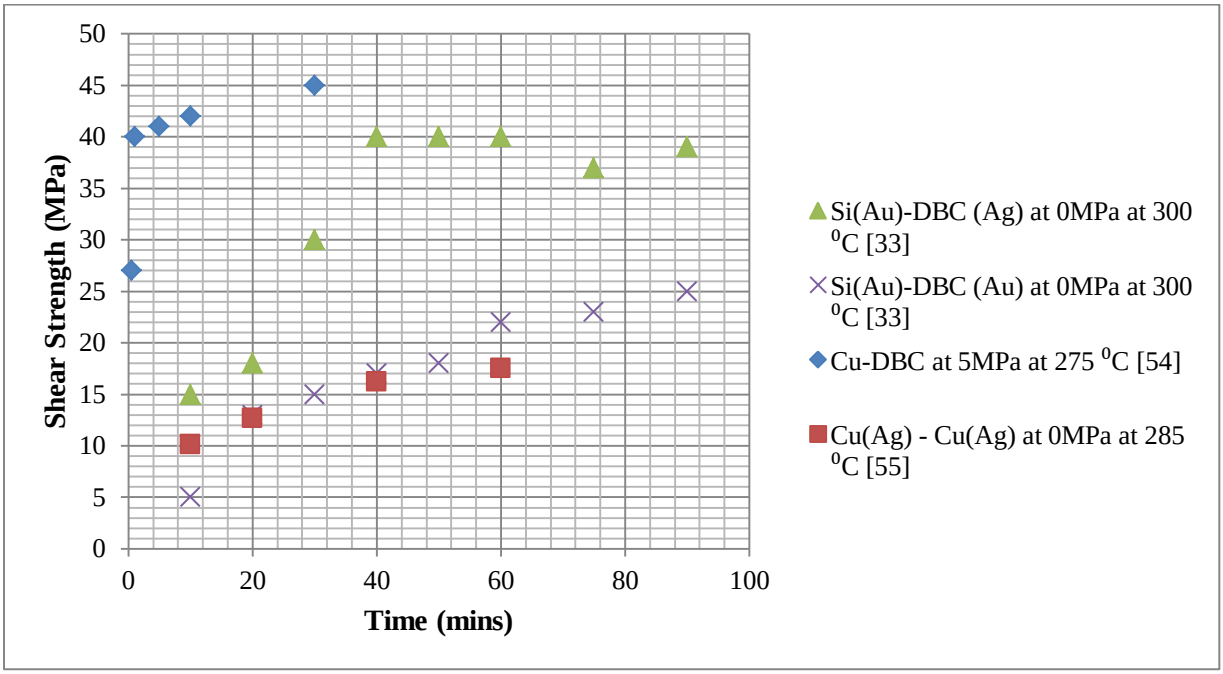


Figure 2.10 The relationship between shear strength of nano silver bonding and sintering time [49]

#### 2.1.4.2.1.3 Heating Rate

The heating rate has an influence on the shear strength of joining with nano silver paste. Increasing the heating rate gives a better and denser sintering joining area. However, to evaporate organic materials in the paste, the heating rate ought to be slow enough to allow. Outgassing of solvents create voids over the bonding line thickness of nano silver paste. As a consequence, it reduces the shear strength and reliability of joining. The recommended heating rate for silver-paste is reported to be approximately 10-20 $^o$C per minute [57].

#### 2.1.4.2.1.5 Substrate and die surface condition

Studies which make use of nano silver paste on bare substrate or die material, i.e. copper, have shown that the shear strength of bonding is weak because of oxidation [58], [59]. Nevertheless, nano silver paste has been successfully used to connect die and substrates coated with Au and/or Ag layers. In some cases, Au and Ag layers are found to be on Ni and Ti layers which are coated directly on substrate/die to act as a diffusion barrier layer. Among the coating layers utilized, Ag coating layer exhibits the best results in terms of better bonding/sintering properties with silver-paste mainly due to the same lattice structures. [57].

#### 2.1.4.2.1.6 Particle Size

Nano particle size inside the paste has an impact on the shear strength as much as sintering temperature and pressure. Figure 2.11 demonstrates the particle size effect on shear strength of various particle sizes (data compiled from [54], [60]). In reference [34], when nano particles are reduced from 100 nm to 10 nm, the shear strength increased six times because of the high surface energy of nano particles. In addition, larger distributions of particle sizes and different particle shapes have better shear strength [57]. Another study reported that micro scale silver particles and nano silver particles are mixed with each other to obtain denser joints [61].

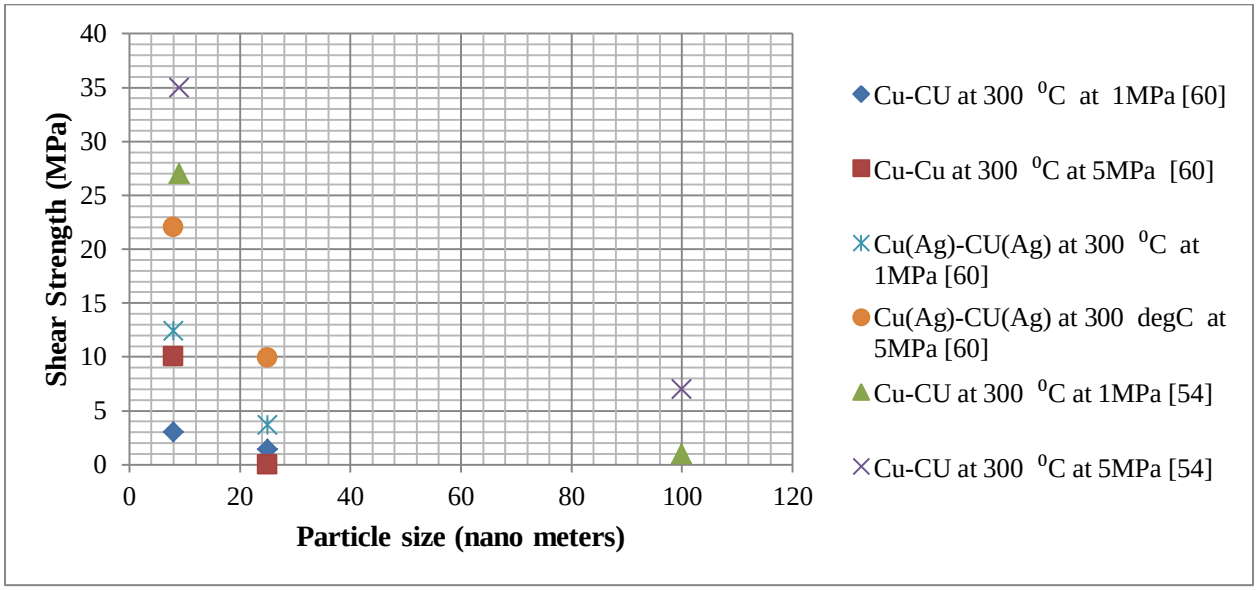


Figure 2.11 Effect of particle size on shear strength of various die attachments [57]

#### 2.1.4.2.1.7 Sintering Atmosphere

During sintering, organic materials are evaporated when temperature increases. Therefore, nano silver particles engage each other. The organic materials passivize these nano particles. Oxidation is necessary for burning out process organic materials inside the paste. Air atmosphere sintering has been reported to have better joining density and higher shear strength compared to a nitrogen environment [62].

### 2.1.4.3 Miscellaneous Fabrication Methods

#### 2.1.4.3.1 Cast Model Sintering

Q. Lu and et al. [63] improved different sintering methods for fast sintering including silver-paste. A rapid current-assisted technology (CAST) was used to bond chip and substrate via nano-silver paste. A schematic illustration of the CAST method is shown in Figure 2.12. Dummy chips and substrates were bonded to each other using nano silver paste when alternative current was applied to two electrodes. The current varied from 5.5 kA to 8.25 kA and the applied time was from 500 to 1000 ms. The applied pressures was changed between 5 MPa to 10 MPa The shear strength varies from 17.8 to 86.5 when the ac was changed between 5.5 kA and 8.25 kA.

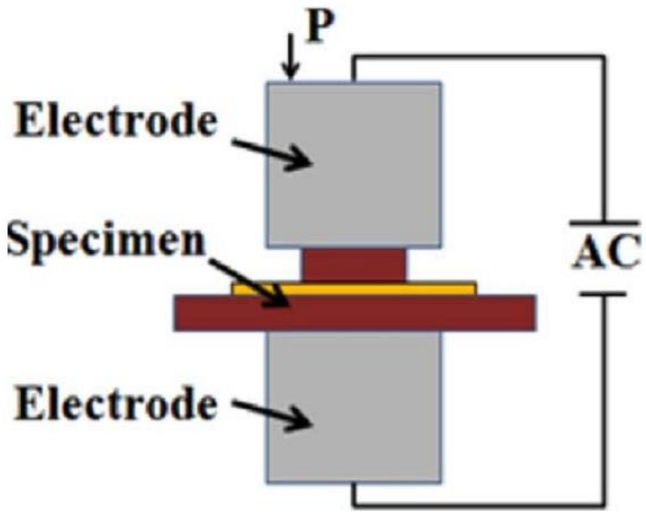


Figure 2.12 A Rapid Current-Assisted Technology [63]

#### 2.1.4.3.2 IR Laser

Lee and et al. studied [64] nano silver paste for LED (light-emitting diode) using a laser as the heat resource. In this method, IR laser, which had a power of 30W and 600 $\mu$m laser beam diameter, was used to increase the temperature of the chip as shown in Figure 2.13. The sample was preheated at 230 $^{o}$C for one minute and the sintering process was completed within 10 seconds at 400 $^{o}$C. The measured shear strength was 8.9 MPa Although the chip area was large, and dimensions reached up to 1.5 mm X 1.5 mm, all the organic materials burnt out despite high preheating temperature. For this reason, the sintering succeeded even if the heating rate was high.

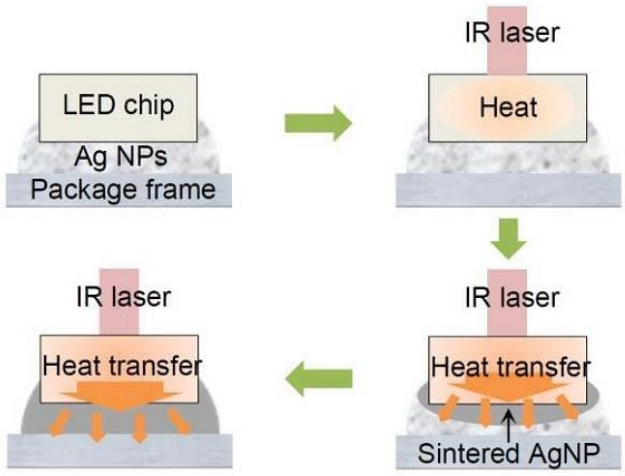


Figure 2.13 Laser Sintering Method [64]

#### 2.1.4.3.3 Ion-Activated Joining

Nano materials are very active because of their high surface energy. The organic materials inside the paste act as a passive layer. When the temperature is increased, this layer is removed and the aggregation occurs between nano particles. This passive layer was removed at room temperature using a chemical solution which consists of NaCl, $MgCl_2$, and $CaCl_2$ [65]. This type of process is called ion activated joining, Figure 2.14

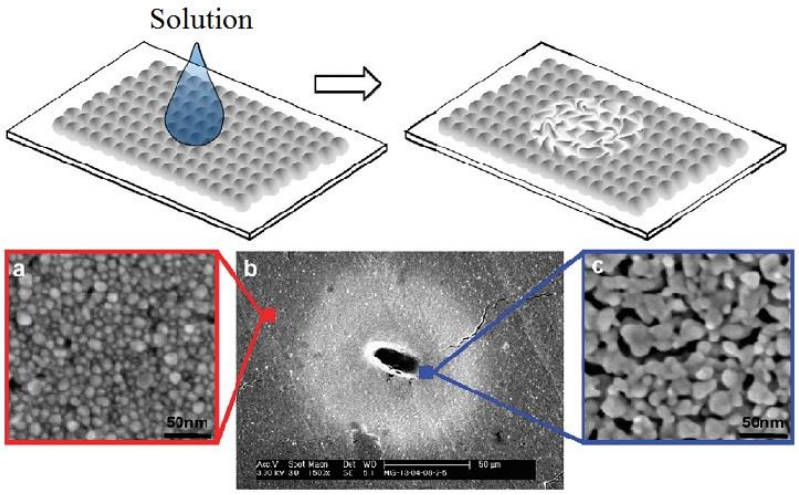


Figure 2.14 Ion Activated Joining [65]

# Chapter 3
# Methodology

In this chapter, materials, manufacturing and characterization techniques utilized throughout the study were described in detail. Section 3.1 gives information about the properties of starting materials while Section 3.2 presents experimental variables and the set-up used during the joining of dummy chips to copper substrates via nano silver paste. Details of the studies including microstructural, mechanical and electrical characterization were given in Section 3.3

## 3.1 Materials

### 3.1.1 Substrates and Dummy Chips

101 super conductive copper, also known as oxygen-free electronic (OFE) or oxygen-free high conductivity copper (OFHC), was chosen as substrate material as it has similar properties to Direct Bonding Copper (DBC) substrate commonly used in IGBTs. 25 mm X 3mm copper 101 flat bars, supplied by McMaster Carr, Aurora, OH had 99.99 % purity. 101 Copper is commonly used for electrical applications, for example, coaxial cables, terminal lugs, and high temperature and vacuum environments. Table 3.1 shows 101 copper material properties.

Table 3.1 Properties of copper 101 used in the study [66].

| **Properties** | **Unit** | **101 Copper (Cu)** |
|---|---|---|
| **Density** | $g/cm^3$ | 8.94 |
| **Hardness** | HRB/HRF | 45/85 |
| **Tensile Strength (Ultimate)** | MPa | 275 |
| **Modulus of Elasticity** | GPa | 115 |
| **Poisson's Ratio** | - | 0.31 |
| **Shear Modulus** | GPa | 44 |
| **Melting Point** | $^oC$ | 1083 |
| **Thermal Conductivity** | W/(mK) | 391 |
| **CTE at room temperature** | $\mu m/m^oC$ | 17 |
| **Electrical Resistivity** | $\mu\Omega$-cm | 1.71 |

Copper parts to be used in joining as substrate material and dummy chips were cut from copper 101 flat bars. Sixty copper substrates were machined to obtain a rectangular shape of 2.5 cm X 4 cm.The thickness was decreased to 3mm and a relatively flat surface was obtained after machining and using successive grinding steps by sandpapers (180, 240, 320, 400, 600, 800, and 1200). Copper was chosen as a dummy chip because silicon is a brittle material and it is reported that silicon specimen is destroyed during the shear strength test due to strong bonding [67]. Likewise, 60 dummy chips (4 mm X 4 mm) were prepared using the same sample preparations steps used for substrates. Next, the surfaces of each group of samples were cleaned with acetone and isopropyl alcohol. To coat copper substrates and dummy ships, a sputtering machine was used. Afterwards, they were coated with silver that was described in Section 3.2.1. Images showing silver coated copper substrate (a) and dummy chips (c) and starting copper substrate (b) and dummy chips (d) (Figure 3.1).

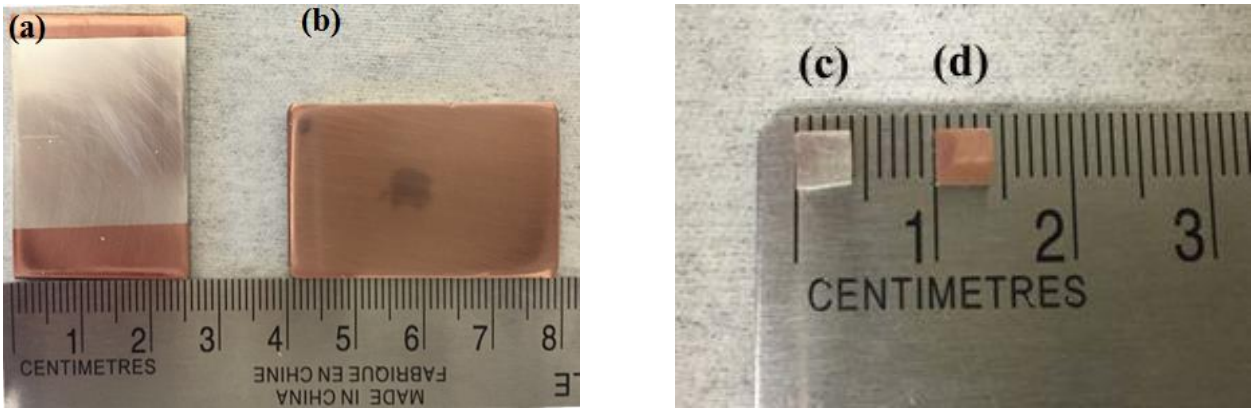


Figure 3.1 101 Images showing (a) silver coated copper substrates, (b) starting copper substrates, (c) silver coated dummy chip, (d) starting copper dummy chip.

### 3.1.2 Quartz Dummy Chips

Quartz has been chosen for electrical measurements of sintered silver because of its non-conductive properties. It contained 99.995 % silicon dioxide. Table 3.2 demonstrates properties of quartz.

Table 3.2 The properties of quartz used in electrical property measurements [68].

| **Properties** | **Unit** | **Quartz** |
|---|---|---|
| **Density** | $g/cm^3$ | 2.65 |
| **Dielectric Constant** | - | 4.2 |
| **Melting Point** | $^oC$ | 1470 |
| **Thermal Conductivity** | W/(mK) | 6.82 |
| **CTE at room temperature** | $\mu m /m\,^oC$ | 8.10 |

Before the application of silver paste, 20 quartz samples were cut from larger discs (thickness approximately 1.7 mm) to obtain 5 mm X 5 mm plates (Figure 3.2) and they were cleaned with acetone and isopropyl alcohol.


Figure 3.2 Quartz dummy chips used in electrical property measurements of sintered silver.

### 3.1.3 Nano Silver Paste

Nano silver paste was received in 25 g containers from NIHON SUPERIOR CO., LTD as shown in Figure 3.3. According to the data sheet given in Appendix B, the average particle size was approximately 10 nm; however, chemical composition was unknown since the company did not share it because of privacy concerns.

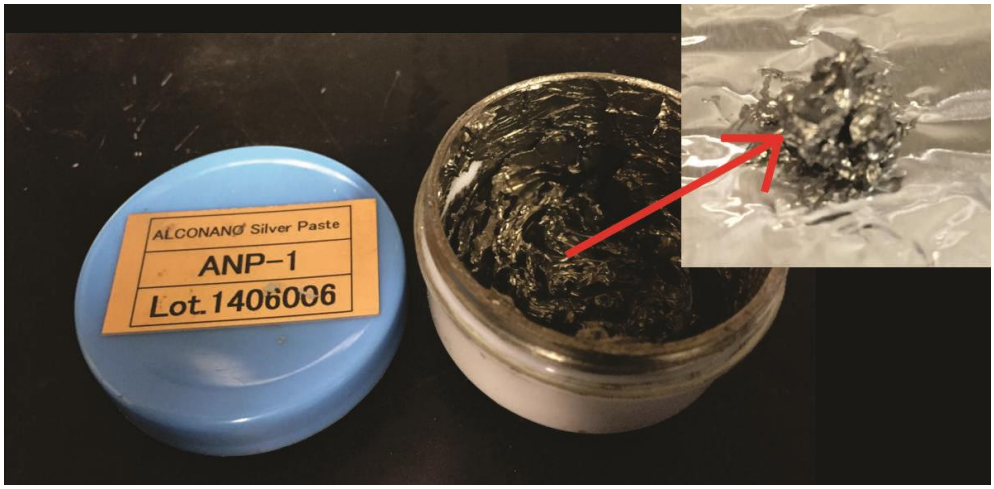


Figure 3.3 As received nano silver-paste.

Scanning electron microscopy (SEM) examination of the starting paste, which was preheated prior to examination at 50$^{o}$C for 10 mins for evaporation of volatiles, revealed mostly spherical nano-particles having diameters as large as 200 nm.

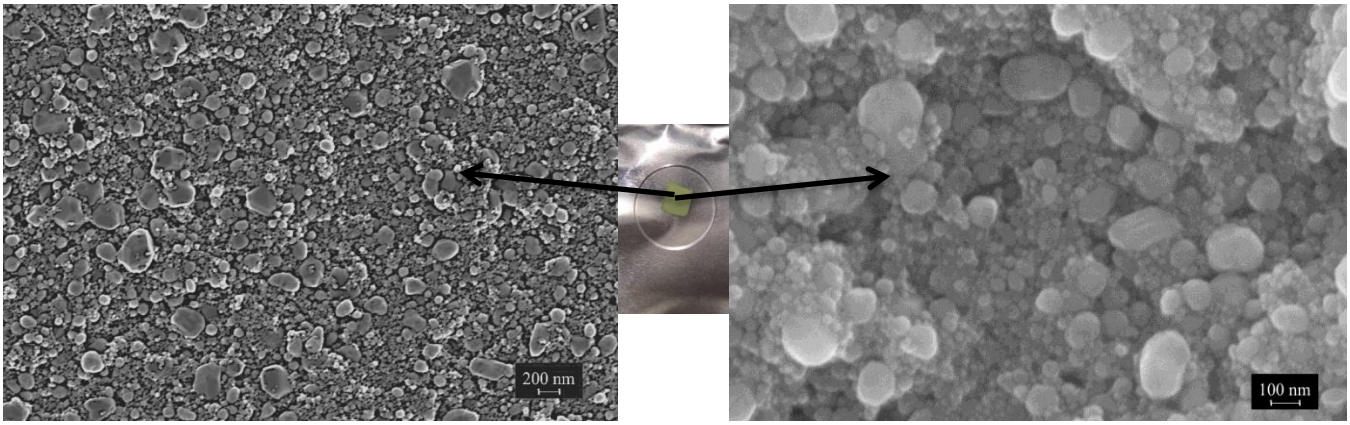


(a) (b)

Figure 3.4 SEM images showing morphology of silver nano powders in silver Paste SEM Images after preheating (a) 18000 X, (b) 52000 X

Energy dispersive X-ray spectroscopy (EDX) examination was carried out on the group D setup sample. The result shows that all organic materials burnt out and only silver remained, in Figure 3.5.

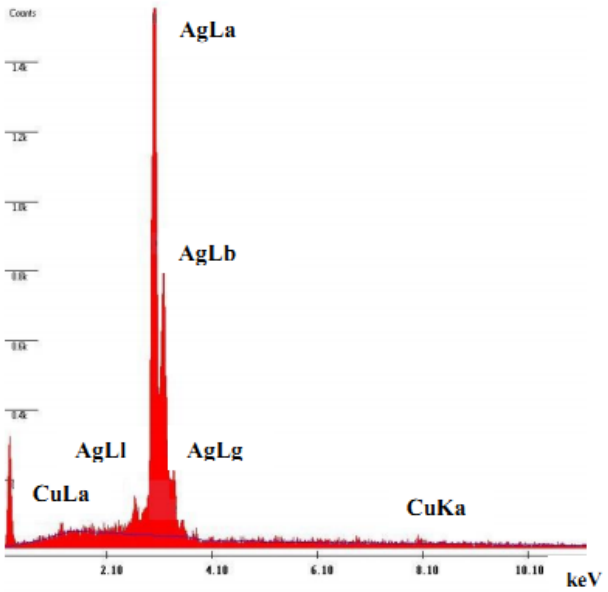


Figure 3.5 Energy dispersive X-ray spectroscopy (EDX) data from air test setup

## 3.2 Experimental Studies

Figure 3.6 shows schematics of production steps. The starting material was copper. Firstly, substrate and dummy chip coated with silver. Secondly, nano silver paste was placed on substrate. Next, binders and organic materials removed with preheating process. The last step, sintering occurred with or without pressure.

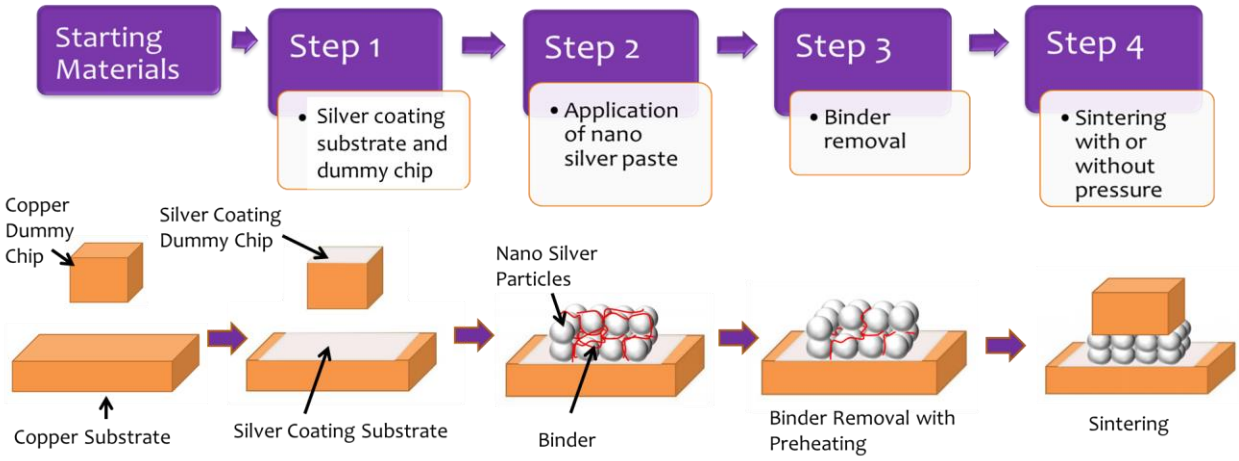


Figure 3.6 Production steps used in the current study

### 3.2.1 Silver coating with Sputtering Technique

To increase sinterability of nano silver particles to substrates and dummy chips, substrates and dummy chips were coated with a thin layer of silver. For this process, a ATC-Orion 5 UHV sputtering machine was used. The sample surfaces were cleared with Argon plasma for two mins, and then the coating process was started. The process took 30 minutes and the thickness of the layer was approximately 500 nm.

### 3.2.2 Application of Silver Paste

After coating the surfaces of copper substrates and dummy chips, nano silver paste was applied on Ag-coated surfaces using screen-printing method. Silk screen with 100- mesh (100 meshes in 1 $cm^2$) was chosen since large mesh size allows the transfer of more materials to the printed surface. For mask screen printing, 3M scotch box sealing tape 311 was used and its thickness was 0.028 mm. Two layers of tape stuck together and a square opening is created at the center of the tape to manage silver paste layer with nano size thickness and 10 mm X 10 mm square to transfer nano silver paste. Substrate placed in a holder and screen-printing was successfully achieved as shown in Figure 3.7.

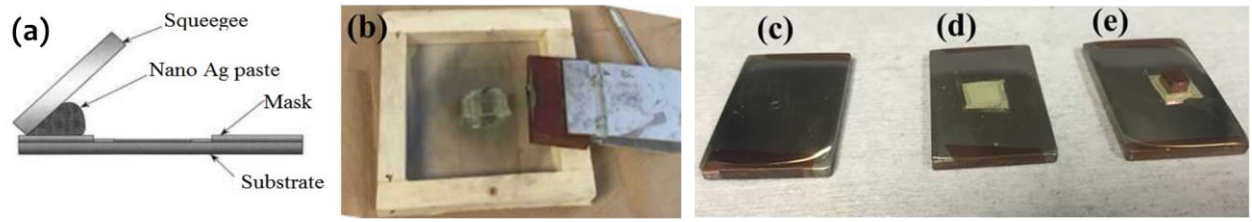


Figure 3.7 Screen Printing Method used in the study (a) Schematics of screen printing method, (b) silk mesh and silver paste at the center, (c) silver-coated copper substrate, (d) silver paste printed on substrate, (e) sandwich structure for joints after preheating**.**

After placing nano silver paste on the substrate, the preheating process was applied to evaporate solvents in the silver-paste. A Corning PC-600D hot plate, which has a 25.4 x 25.4 cm Pyroceram top and digital temperature display, was used. Preheating temperature was 50 $^{o}$C for 10 minutes. During this process, the paste color changed from dark to light greenish.

### 3.2.3 Joining process

During the joining of two copper parts, namely, substrates and dummy chips, with nano silver paste, three different pressure-assisted fabrication methods were used to obtain five different groups of samples (Groups A, B, C, D and E). For the production of group A and B samples, a flip chip machine was used to apply ultrasonic force. On the other hand, a specially designed fixture was used in a vacuum and air environment for production of Group C and D samples. Joints in this group were preloaded using a metallic screw. For group E, a pneumatic system, capable of maintaining constant pressure, was used during fabrication in air. The details of the set-ups used for production will be given in the following sections. Table 3.3 represents the variables used during production of each group of samples. Production of each group was composed mainly of 3 stages, namely, preheating for evaporation of volatiles, sintering of silver nano particles and cooling down to room temperature.

Table 3.3 Variables used in the joining process of various groups using silver nano-paste.

| Test Group | Sintering Atmosphere | Pressure During Heating Stage (MPa) | Pressure During Sintering (MPa) | Additional Force and Condition | Sintering Heat Treatment Cycle |
|---|---|---|---|---|---|
| **A** | Air | 0.01 | - | - | Given in Figure 3.8 |
| **B** | Air | 0.01 | - | 0.3 Watt ultrasonic force | Given in Figure 3.8 |
| **C** | Vacuum | 5 | 5 | Gradual pressure decrease during sintering | Given in Figure 3.10 |
| **D** | Air | 5 | 5 | Gradual pressure decrease during sintering | Given in Figure 3.10 |
| **E** | Air | 5 | 5 | Constant pressure through the sintering | Given in Figure 3.12 |

#### 3.2.3.1 Group A and B samples

The dummy chip was placed onto dried nano silver paste after the preheating process was completed. Group A and B samples were produced using almost the same processing variables except for the ultrasonic force which was only used during Group A sample production. After preheating, an ultrasonic force at 0.3 W was applied using JFP Microtechnic DB 5 flip chip bonder. The flip chip bonder had a 10 mm X 10 mm maximum die size holder with two CCD cameras and it was capable of applying 60-65 kHz horizontal ultrasonic force and 200 grams bonding load force. Therefore, a maximum load of 200 g was applied to both groups during heating to sintering temperature in air with a heating rate of 11.25$^{o}$C, Figure 3.8. Then, samples were sintered for 30 minutes at 275 $^{o}$C for 30 mins after removal of the load. Subsequently, samples were cooled down to room temperature naturally.

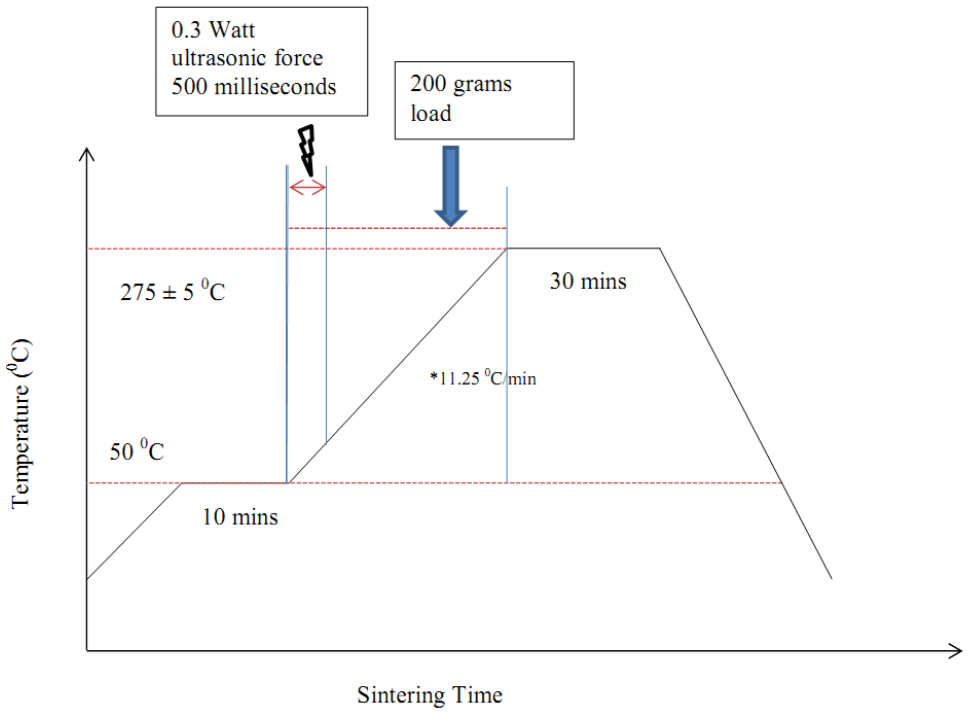


Figure 3.8 Preheating and sintering cycles used for the production of Group A and B samples.

### 3.2.3.2 Group C and D samples

As presented in Table 3.3, Group C and D samples were produced in a vacuum and air atmosphere, respectively, using the fixture shown in Figure 3.9. The force was applied with a metallic screw prior to preheating and sintering only, and it could not be controlled and maintained constantly during each production step due to lack of a pressure controller in the design. Initially, the corresponding force for each turn of the screw was measured and calibrated with a load cell and then samples were preloaded at 5 MPa.

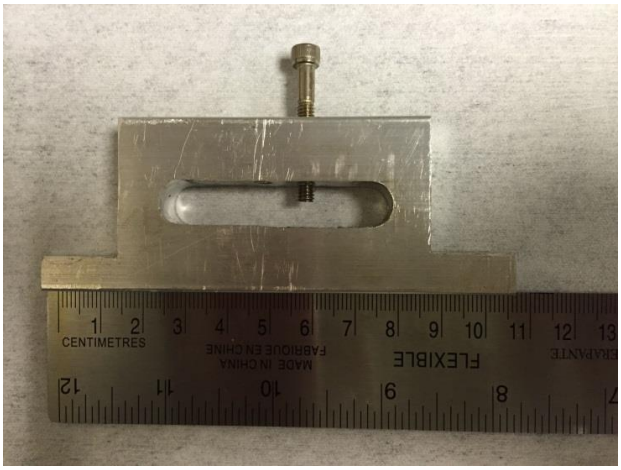


Figure 3.9 Fixture used to apply pressure via screw during production of Group C and D samples.

The specimens (Group C) were placed in a vacuum chamber after being preheated at 50°C for 10 minutes. When the vacuum chamber reached 0.3 mbar, the heating stage was turned on and samples were heated to sintering temperature with a heating rate of ~11.43 ° C /min. After the temperature reached 275 ± 5 ° C, sintering was conducted for 30 mins, Figure 3.10. Samples were taken out of the heating stage when they cooled down to room temperature. Similarly, Group D samples were produced using the same processing variables; however, sintering atmosphere was air instead of vacuum.

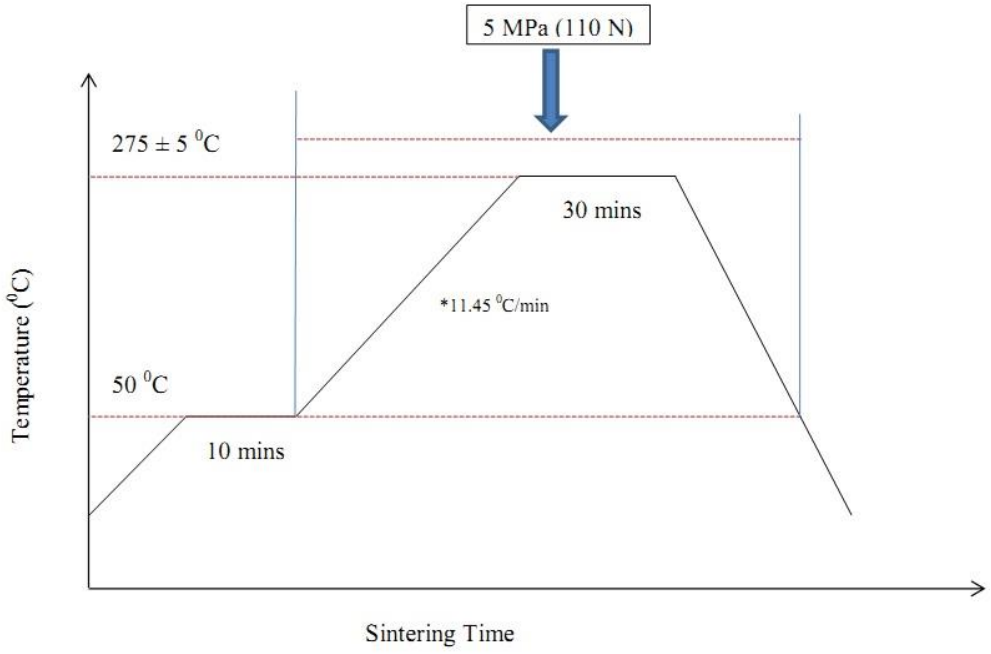


Figure 3.10 Preheating and sintering cycles used for the production of Group C and D samples.

### 3.2.3.3 Group E samples

The sandwich structure was mounted into a pneumatic system to apply pressure. The system consisted of a pressure regulator, a digital gauge, a compact flexible-mount air cylinder with 100 mm diameter piston, and high pressure air hose as shown in Figure 3.11.

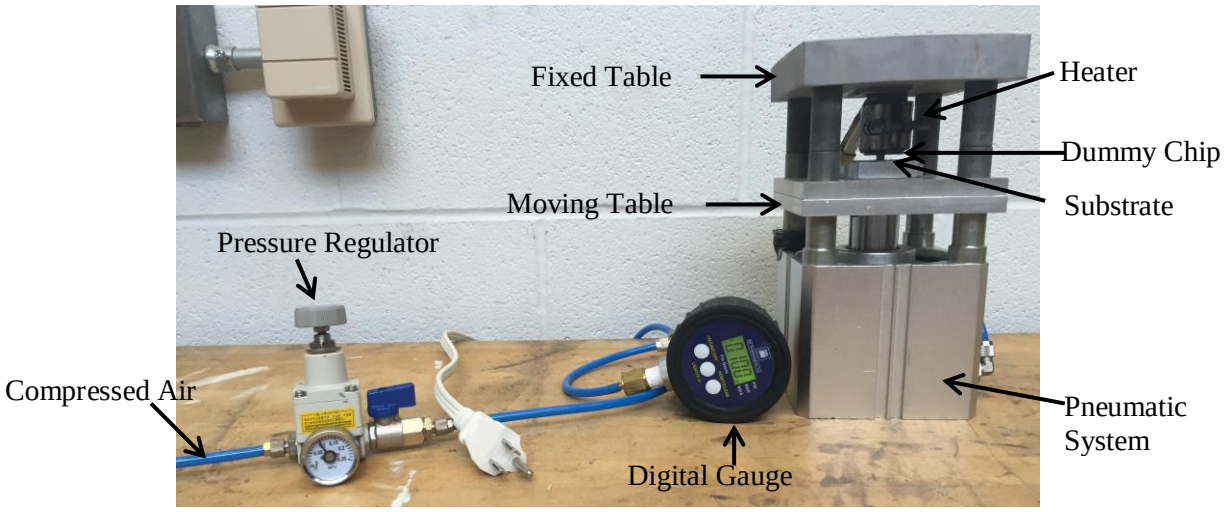


Figure 3.11 Constant Pressure Fixture

To adjust the pressure during production, the digital gauge value was multiplied by the ratio between the piston area in air cylinder and dummy chip area. For example, if a dummy chip connection area is 16 $mm^2$, and the piston area is 7857.1429 $mm^2$, the ratio between these areas is 491. To obtain 5 MPa pressure during production, the digital gauge value was adjusted to 0.01 MPa.

After a preheating step as described previously, the samples were heated to sintering temperature, 275 ± 5 $^{o}$ C, with a heating rate of 11$^{o}$C/min and held at this temperature for 30 mins. After the sintering process was completed, the samples were cooled down to room temperature. During the whole sintering cycle (heating, holding and cooling), pressure was maintained almost constant automatically by the pneumatic system. Figure 3.12 shows the sintering cycle during the production of Group E samples.

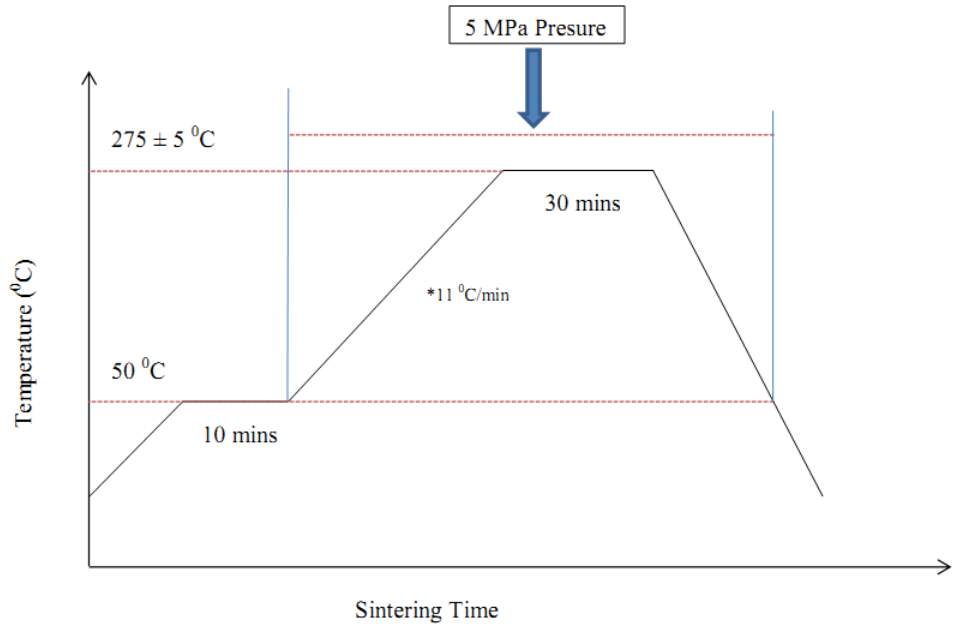


Figure 3.12 Preheating and sintering cycles used for the production of Group E samples.

## 3.3 Characterization Studies

In this section, the techniques used for structural and functional characterization of sintered nano silver joints were presented.

### 3.3.1 Microstructural Examination

For preparation of molded specimens, a hot thermo-setting phenolic resin was used. Mounted samples were obtained using the Labo Press at 200 °C temperature and 50 kN pressure. The grinding process was used to remove the damaged or oxidized layer present on the surface. Firstly, a belt surface grinder machine was used to eliminate residual resin on the sample surface. Specimens were held tight and a low pressure was applied towards the sandpaper. During the grinding process, water was used for cooling and lubricating. Samples were rotated by 90° for each grinding step to completely remove scratches formed in prior steps. The grinding was completed in six steps by using six different sand emery papers with 240, 320, 400, 600, 800, and 1200 grit sizes.

For examination of microstructure under an optic microscope and a scanning electron microscope (SEM), polishing was used to obtain a flat, defect-free surface. Specimens were polished with aluminum oxide solution ($Al_2O_3$) using a Buehler variable speed polishing wheel. Two different solutions were

used. They contained different aluminum oxide powders, which had average particle sizes of around 1 and 0.5. $\mu$m. Polished surface of a specimen is shown in Figure 3.13.

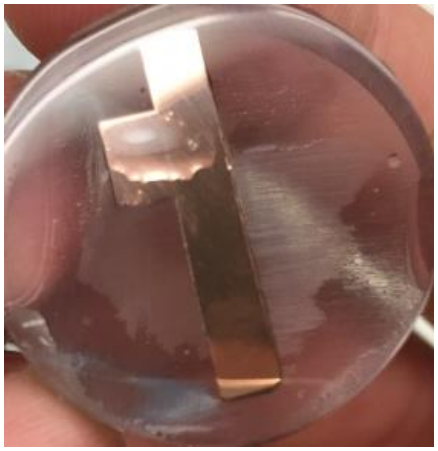

Figure 3.13 Surface of a sample cross-section after polishing.

Ancansco Inverted Metallurgical optic microscope and high resolution LEO 1530 FE-scanning electron microscope (SEM) were performed for microstructural examination. SEM was capable of sub-nanometer resolution; -detectors: In-Lens, SE, and BSE -capable of up to 6" wafer -operational voltage 0.2-30kV -low voltage for viewing non-conductive samples x/y/z axes motorized stage. Its rated resolution was 1.2 nm at 20 kV..

### 3.3.2 Mechanical Characterization

The mechanical properties of joints were tested under shear force using an Instron 4465 500 kg tensile test machine at a cross head speed of 0.5 mm/min. A specially designed fixture was used as shown in Figure 3.14 to create shear force upon application of tensile force

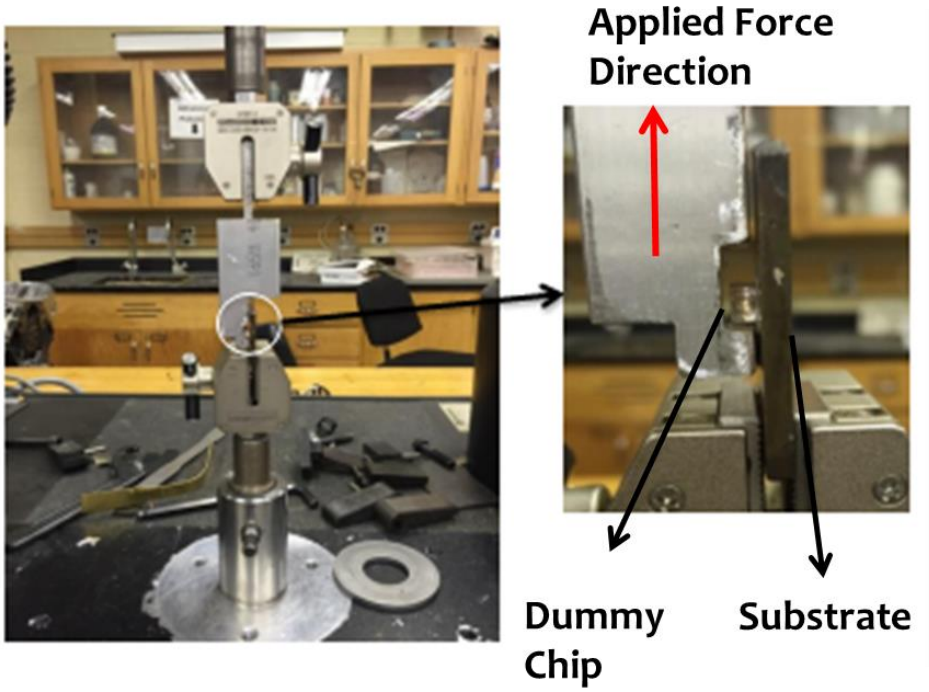


Figure 3.14 Mechanical characterization set-up used in the study.

### 3.3.3 Thickness Measurement

The sintered silver layer thickness was monitored by a Dektak 8 stylus profilometer. The Dektak 8 characterizes film thickness, roughness, stress and defects on samples up to 200mm (8 inches) in length. The system has low-force tip technology, long-scanning capability and versatile data analysis software. The thickness of sample was measured electromechanically by moving a diamond-tipped stylus. It is computer-controlled and programmable [69].

### 3.3.4 Electrical Characterization

5 mm X 5 mm quartz dummy chips and 1 inch diameter quartz substrates having 1.7 mm thickness were used for resistivity measurement of sintered silver nano-particles. Quartz was preferred to hold the sintered particles because of its non-conductive and non-reactive properties in the sintering temperature range. After fabrication was completed, quartz plates could be separated from each other easily and a uniform sintered nano silver layer could be obtained for electrical measurements.

Before the measurements, initially, nano silver paste was placed on glass substrate by screen-printing methods. The thickness of nano silver paste was as same as the thickness obtained in copper specimens.

Preheating was applied at 50 $^{o}$C for 10 minutes as with previous samples and the same sintering profile and pressure was applied for each test condition.

After naturally cooling the samples down to room temperature, the quartz substrates and quartz dummy chips were separated from each other. During the separation process, sintered silver-paste layer was lifted up easily from one part and remained only on the other part, either on quartz substrate or on the quartz dummy chip. Then, the sintered nano silver layer's sheet resistivity was measured using Resistivity Test Rig, Model B, A & M Fell LTD four probes device. The current was applied outside two probes and the voltage was measured internal two of these four probes. The sheet resistance was calculated from the measurement results using the following equation:

$$R_{sheet} = C_f \frac{V}{I} \tag{3.1}$$

where $C_f$ is a geometric correction factor, V is the measurement value of DC voltage across the inner two probes and I is the applied DC current passing through the outer of these four probes. This correction factor depends on the sample size and probe spacing. For the sheet resistance measurement, since layer thickness of sample (t) was much smaller than spacing distance between the probes (s) (t<<s), the correction factor was assumed to be $\pi/\ln(2)$, which is around 4.5324 [70]. At least 10 different points were measured for each sample and the average value calculated as the sintered silver layer sheet resistance. The electrical resistivity of sintered layer was calculated by multiplying the layer thickness by the layer measured sheet resistivity (Equation 3.2).

$$\rho = t \,.\, R_{sheet} \tag{3.2}$$

# Chapter 4
# Results and Discussion

In this chapter, firstly, microstructural examination of sintered silver joints manufactured via various processing routes was presented. Then, quasi-static mechanical responses of joints under shear loading were given in the following section. Moreover, microstructure and mechanical property relations are discussed, considering porosity and sintering necks in the aforementioned joints. Likewise, electrical properties, i.e. resistivity, of joints were compared and contrasted considering the microstructure developed after each joining process.

## 4.1 Microstructural Examination

Figure 4.1 displays the cross-sections of joints after using various joining processes for Group A-E samples presented in Table 3.3. The sintered joints exhibited mainly two different cross-sections, namely, non-uniform joints with micro porosity and continuously well-bonded porosity-free joints. Although the sintered porous silver interfaces in some joints (Groups A-C) were comparatively thicker, Figure 4.1 (a)-(c), thinner sintered silver regions were observed in other samples (Groups D, E), Figure 4.1 (d), (e), indicating better sintering and a high degree of shrinkage.

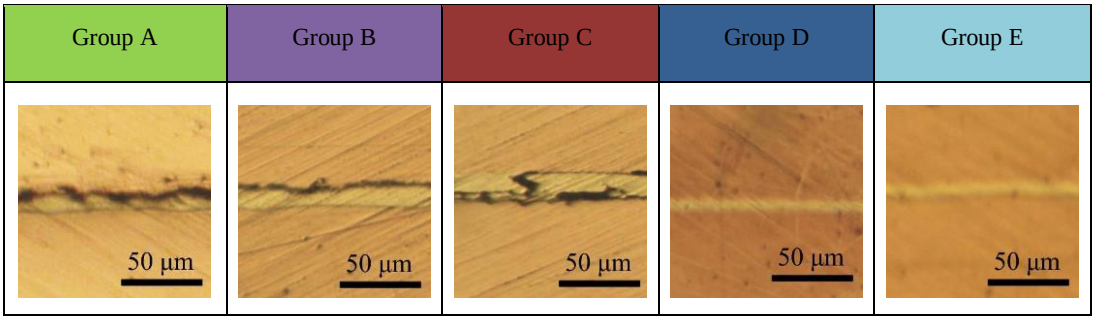


Figure 4.1 Micrographs of cross-sections in various joints formed by different processes.

Figure 4.2 presents the representative SEM micrographs of joint cross-sections with and without porosity and micro-cracks. Partial fracturing and residual porosity in the interfaces shown in optical micrographs (Figure 4.1) has been observed to occur especially in the layer separating silver coating from the sintered silver nanoparticle region, Figure 4.2 (a). Micro fracture at the interface indicates partial bonding between the layers probably due to a smaller available sintering surface for silver nanoparticles. The appearance of such defective interfaces was attributed to insufficient pressure applied during the heating and/or sintering stage. On the other hand, very good bonding was seen in the interface region

between copper, silver coating and sintered-silver nanoparticle regions in Group D and E samples, Figure 4.2 (b).

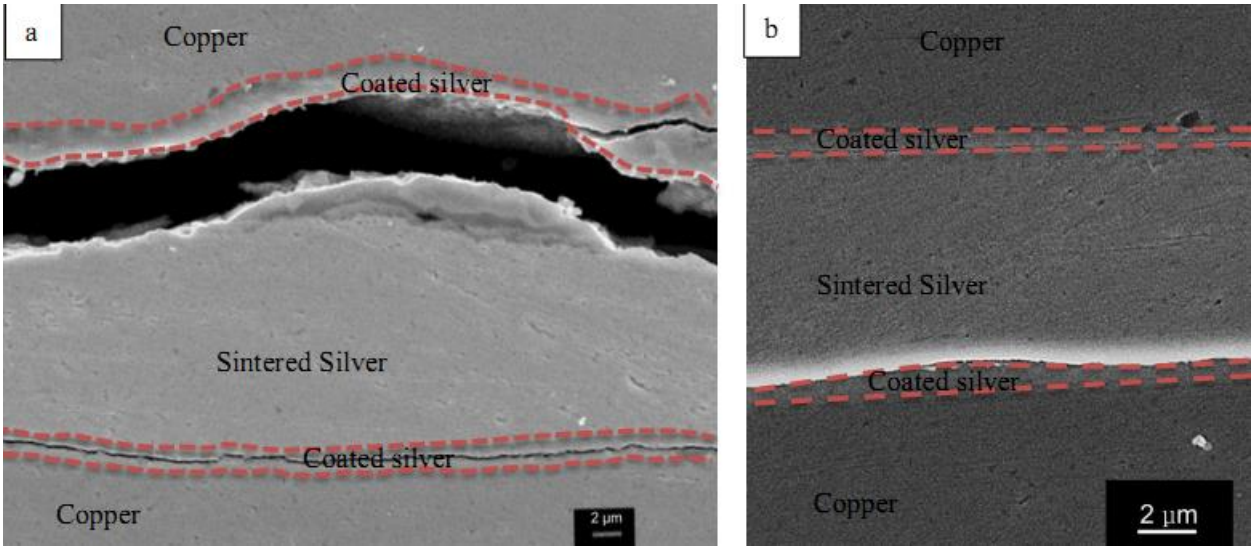


Figure 4.2 SEM micrographs showing representative cross-sections of samples containing micro-crack and porosity and porosity free samples, (a) Group A, (b) Group E.

Microstructures shown in Figure 4.3 demonstrate the degree of sintering between nano silver particles for each test condition in sintered silver regions of the joints. Microstructural examinations revealed that the joining process at constant pressure in air resulted in the highest density and shrinkage with relatively high neck size ratio, X/D (X: neck size, D: particle diameter), while the bonding between silver nano particles was relatively loose especially in those joined without ultrasonic force (Group A). Similar sintering behavior was also observed in Group B and C samples produced using ultrasonic force and vacuum; however, they exhibited better sintering with less porosity compared to Group A. Although micro porosity left due to insufficient sintering was detected in all samples regardless of the joining technique, large residual macro pores were observed especially in Group A, B and C samples as shown with arrows in Figure 4.3 (a)-(c).

The reason for the presence of residual macro and micro pores between silver nano particles is twofold. One of the possible reasons is the lack of sufficient pressure, which is needed to create the available surface for diffusion. It is known that higher interfacial area or higher numbers of contacts occurs

between the nano silver particles and between the nano particles and substrate material as well. Moreover, the pressure helps in the rearrangement of the nano silver particles to form higher packing density, align the grains and eliminate most of the macro pores in green compact [49]. Therefore, application of higher pressure and maintaining it constant throughout the sintering process is crucial in terms of obtaining high shrinkage and high density powder metallurgy products. Accordingly, residual porosity in Group C, D and E samples was relatively lower because of higher pressure applied, i.e. 5 MPa, Figure 4.3 (c)-(e). The quantity of porosity was even lower in Group E samples as the pressure was maintained constant during sintering. On the other hand, 5 MPa pressure applied in Group C and D was treated as a kind of preload since it is created via screws and it gradually decreased during sintering.

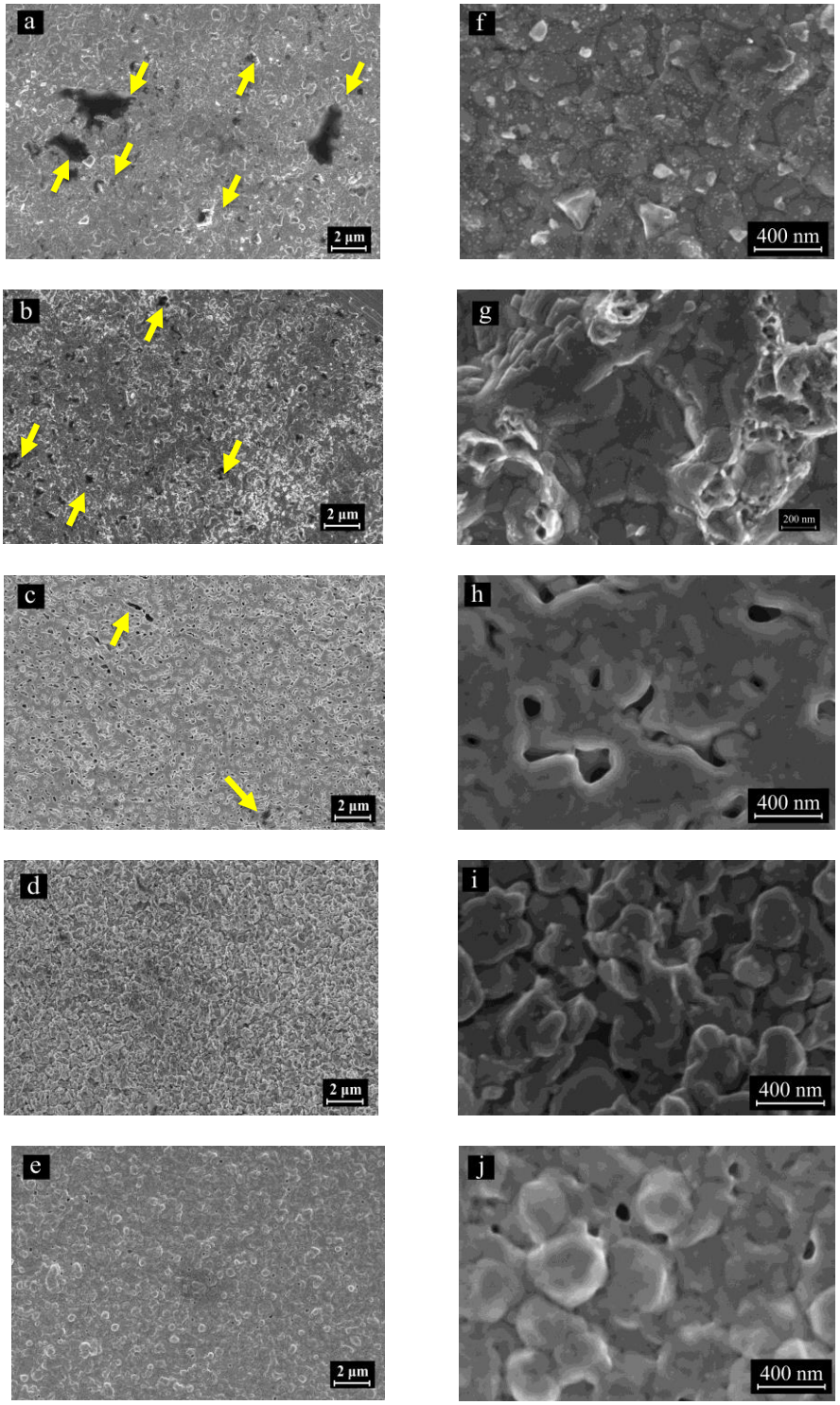


Figure 4.3 SEM micrographs of sintering surfaces of sintered nano-silver joints (a) and (f) Group A, (b) and (g) Group B, (c) and (h) Group C, (d) and (i) Group D, (e) and (j) Group E E

Sintering can be described as a mass transport process and the system tries to decrease surface energy by eliminating or decreasing the surface area. Between two particles, possible diffusion routes are illustrated in Figure 4.4 during sintering. Surface and lattice diffusion occur over route 1 and 2. Usually surface diffusion results in the formation of sintering necks without densification. On the other hand, grain boundary and through-lattice diffusion result in significant shrinkage and densification. These atomic diffusion events require different amounts of energy. During the initial sintering stage, surface diffusion is more dominant due to the requirement of low activation energy. For grain boundary diffusion, the required activation energy is lower than that of lattice diffusion but higher than that of surface diffusion. Therefore, through-lattice diffusion and grain boundary diffusion occur at relatively higher temperatures and result in significant densification [71]. For almost all the transport mechanisms, the surface condition of the powders, presence of organics, and the presence of pressure during sintering are important for increased mass transport.

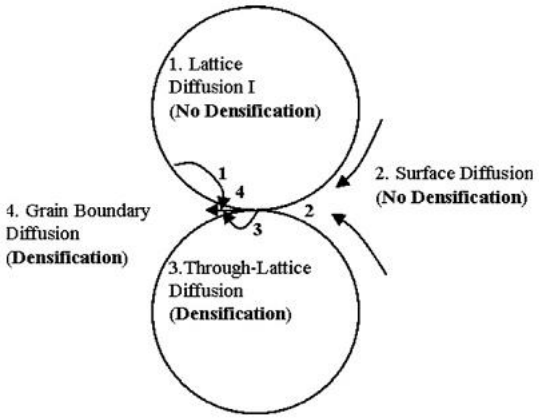


Figure 4.4 Demonstration of various atomic diffusion routes between two silver particles; route 1 is lattice diffusion, route 2 is surface diffusion, route 3 is through-lattice diffusion and route 4 is grain boundary diffusion [71].

As well as the pressure, sintering atmosphere and sintering temperature and time is effective in enhancing the diffusion rate, thereby decreasing the residual porosity. Thus, in the current study, the second possible reason for residual porosity was considered to be sintering atmosphere. If sintering is carried out in vacuum, the degree of sintering is increased due to elimination of possible oxide layers on the particles, which act as a barrier for diffusion of host atoms. Moreover, trapped gas between the particles remaining in the final stage of solid state sintering, Figure 2.4, is eliminated in this way. However, the results of vacuum sintering in the current study were opposite to expectations and the

porosity was relatively higher. Since the silver paste contained some organic materials, which needed to burn out completely, vacuum atmosphere prevented its removal due to limited burn-out. Therefore, the sintering event was degraded due to depletion of the organic materials between the nano particles. When sintering occurred in vacuum, this removal of organic materials by oxidation through heating was not completed owing to the lack of oxygen. Accordingly, the possible organic material residue was considered to be the reason for insufficient sintering and it created micro porosity, Figure 4.3 (c). The air environment, on the other hand, during sintering allowed efficient burn-out of binders and organics, thereby inducing better densification in silver joints.

In addition to utilized atmosphere, the magnitude and duration of the applied pressure also affect the removal of organics and binders. It helps excessive organics flow out of the powder pack prior to sintering and thus, decreases the severity of organics burn-out problems. Moreover, sufficient pressure prevents swelling of the compacts due to evolution of gases during burn out [49]. The effect of pressure on swelling and densification can be seen more clearly in Figure 4.5. Figure 4.5 (a) shows micro porosity with red dots in group A samples which experienced 0.01 MPa during the heating stage. Nano particles were sintered well in some regions only; while most of the regions were composed of voids created due to organics burn out. These voids prevented the contact and diffusion between silver nano particles themselves and the copper substrate. On the other hand, it is observed that the amount of porosity in sintered silver in group E was significantly reduced and the microstructure was more uniform, which had a positive influence on the properties of joints, Figure 4.5 (b), because of sufficient sintering pressure.

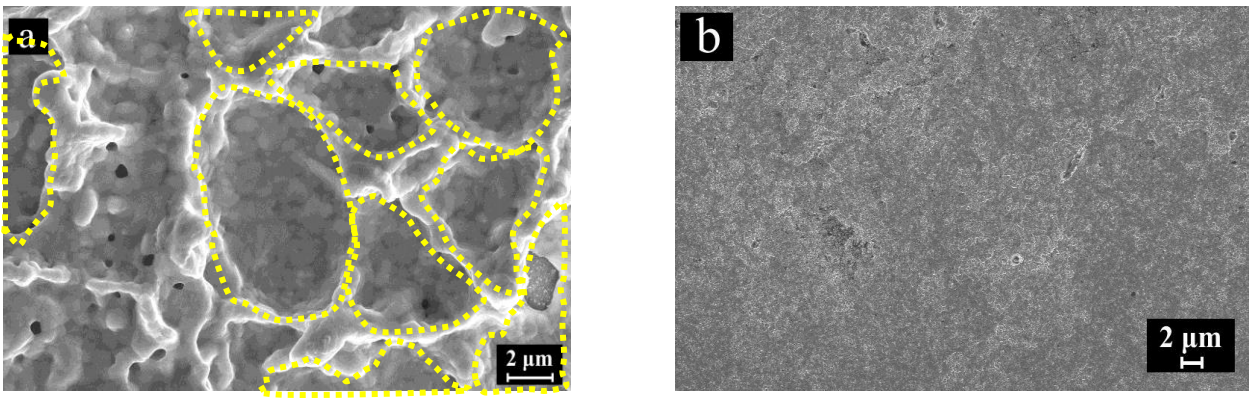


Figure 4.5 SEM image showing the effect of pressure on organics related swelling in (a) Group A samples, (b) Group E samples.

## 4.2 Mechanical Properties

### 4.2.1 Stress-strain curves

As mentioned in Chapter 2, the die-attach materials always face the stress induced due to a mismatch of CTE values of layers. Thus, production of joints capable of withstanding relatively higher stresses makes possible usage of them at elevated temperatures safe and without failure. In the current study, the mechanical properties of sintered nano silver joints in Group A-E samples produced by various techniques were characterized by quasi-static shear tests.

Figure 4.6 shows the stress – strain curves of joints under shear loading. Samples exhibited stress – strain curves similar to wrought alloys having linearly elastic regions, strain hardening up to peak stress and fast fracture after a peak stress. Small strain hardening regions and sudden fracture after peak stress were common characteristic features of the material which indicated brittle-like behavior possibly due to oxidation and/or insufficient sintering. The dominance of each elastic and plastic region was observed to be different in samples joined using different methods. Although group E samples showed relatively lower strain hardening, the remaining samples had comparatively higher strain hardening regions. The strengths of the joints were observed to be highest in Group E samples and it decreased in the following order: Group D, C, B, A. On the other hand, it was difficult to evaluate the elastic moduli of the joints due to lack of an extensometer during testing. Therefore, any relation between elastic moduli and joining technique could not be obtained although elastic moduli is highly affected from the porosity left due to partial sintering across the joint region.

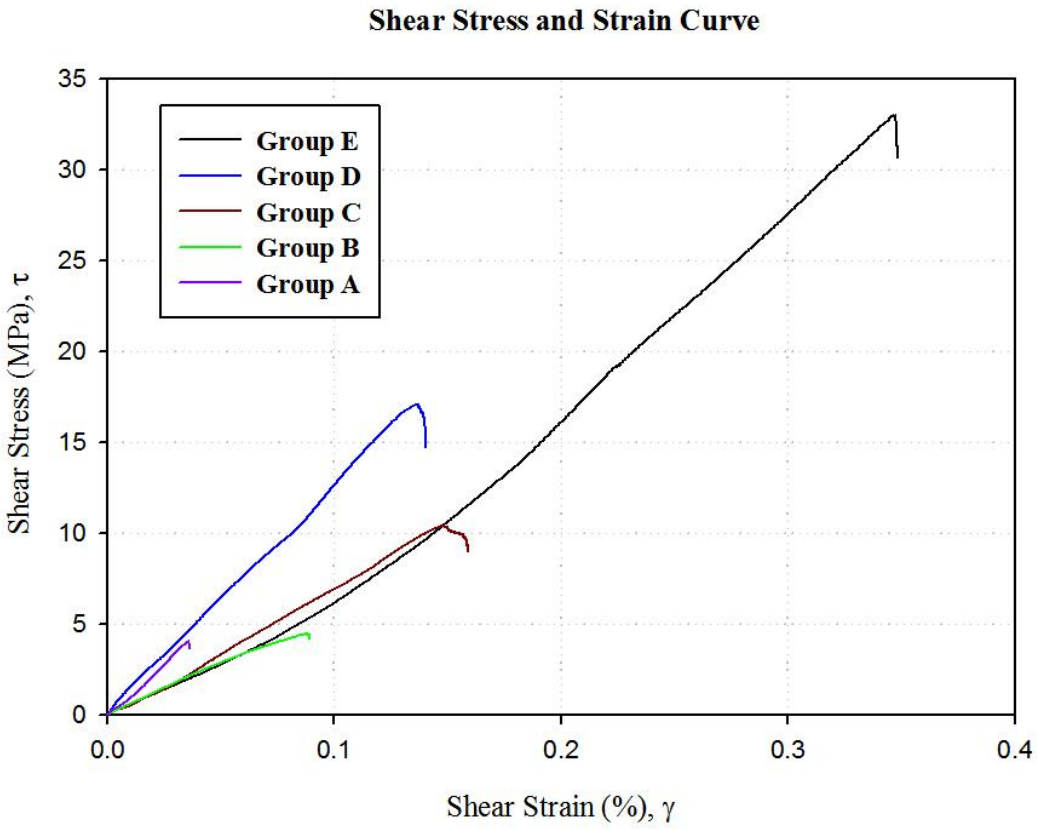


Figure 4.6 The shear stress and strain curve for all test conditions

### 4.2.2 Fracture Surfaces

Examination of the fracture surfaces of joints, Figure 4.7, revealed both the type of fracturing and voids formed as a result of entrapped gases formed during organics removal. In contrast to stress-strain curves, a ductile type of fracture was observed in fracture surfaces due to the presence of dimples. Failure in the samples appeared by tearing of the sintering necks between the nano particles and fracture surfaces smeared in the direction of applied shear stress. As expected, fractured areas or previously sintered regions were higher for Group C, D, E samples manufactured by the application of higher pressure. On the other hand, relatively high density of large voids was observed in Group A and B samples where the applied pressure during joining was lower. The fracture surface was similar to closed cell foams in which each cell is seperated with solid material. These porosities and voids formed during the burn-out of organic materials present in the starting silver paste. Gases which were burning by-products of organics possibly were not able to escape from the bonding area due to lack of persistent pressure during sintering. The porous structures of the joint connected with micro-voids during the shear loading.

The fracture in Group A and B samples propagated mainly through sintered nano silver particles and partially occurred in the interface between sintered nano silver particles and silver coated copper. Although plastic flow (white arrows in the figures) can be observed at all the SEM micrographs in Figure 4.7 (f) and (g), the plastic deformation in the joint with and without ultrasonic force assisted is less evident and less uniform than that in the joints with the other groups. Thus, weak bonding was obtained. This observation is consistent with the measurement of the shear strength of the nano silver joint in group A and B as seen in stress-strain curves. When pressure was increased from 0.01 MPa to 5 MPa for group C, D and E samples the sintered or fracture area increased significantly, Figure 4.7 (h)-(j).

Therefore, it can be concluded that the failure type of the samples was mainly dependent on the mechanical properties of the sintered nano silver layer.

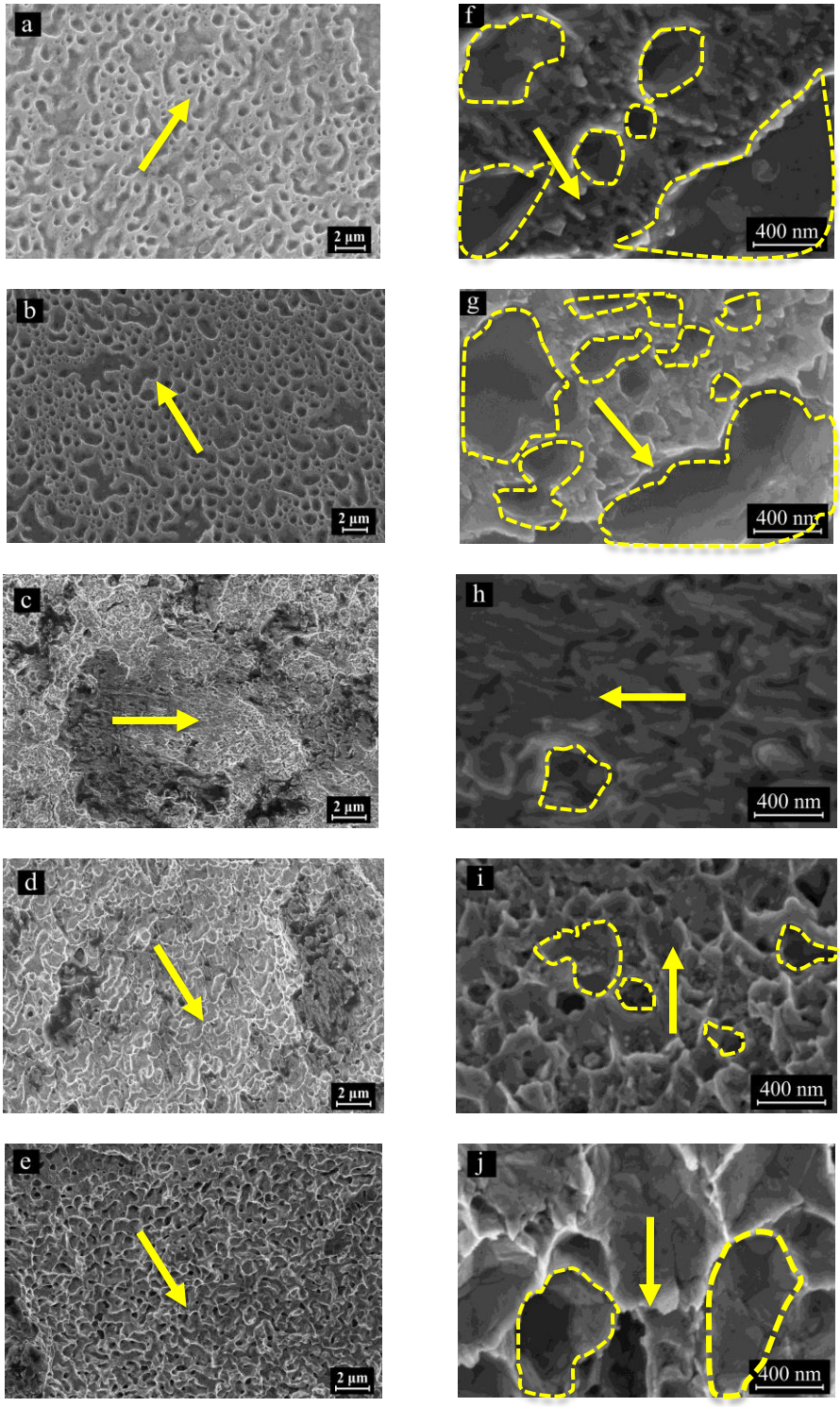


Figure 4.7 SEM micrographs of fracture surface of sintered nano-silver joints (a) and (f) Group A, (b) and (g) Group B, (c) and (h) Group C, (d) and (i) Group D, (e) and (j) Group E

It may also be observed that a more apparent tearing ridge, at which each region is labeled with red dotted lines, and a larger plastic deformation, at which each region is labeled with an arrow, was apparent in the deformed samples under shear loading for group D and E in Figure 4.8 (a) and (b), respectively. It is not only indicative of a more uniform sintered silver layer, but also might be characterized as having a more ductile structure like other metal materials [72].

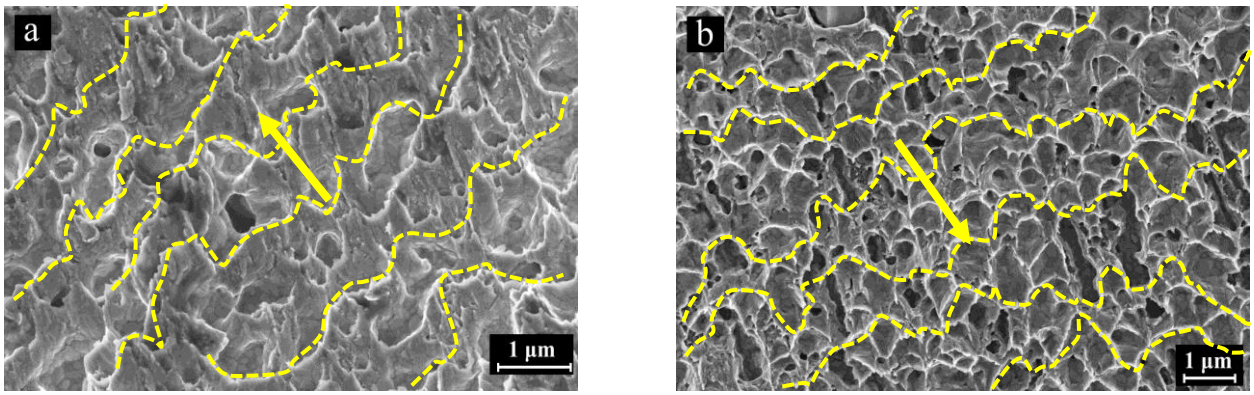


Figure 4.8 Microstructure of fracture section with tearing ridge mechanism and plastic flow for group D (a) and group E (b)

### 4.2.3 Mechanical Properties

There are various models proposed to define the dependence of mechanical properties of sintered parts and porosity parts. Among the empirical models, minimum solid area model has been utilized for indexing the mechanical properties of sintered parts.

In the model, area (actually load carrying area which are the sintering necks) normal to the stress is considered influence on the transmission of stress through the sintered part. Therefore, well sintered parts with larger necks between nano particles are anticipated to have higher strength since localization of deformation appears contacts or necks. The relative mechanical properties of porous samples, such as stress ($\sigma^*/\sigma_o$), are related to the proportion of the total cross section normal area to the stress axis ($A^*/A_o$) in the model [73]–[76]as given in Equation 4.1.

$$\frac{\sigma^*}{\sigma_o} = \frac{A^*}{A_o} \tag{4.1}$$

where σ and A stand for stress and area. On the other hand, superscript "*'' and subscript "o'' defines the sintered samples and bulk counterpart of the same material. The minimum solid area model is a simple estimation of the real sintered area (neck and cross-section area). It shows the sintered samples in loose or compacted condition.

The calculated strength values of the sintered joints were observed to be consistent with the proposed MSA models such that Group A samples which had relatively less load carrying area or small sintering necks exhibited low strength while the stress transfer capacity of well sintered Group E joints was the highest. Figure 4.9 shows the average shear strength values of the samples which was calculated by testing at least 4 samples.

The bonding strength for joints were similar and observed to change approximately 4.1 and 4.4 MPa, respectively, for Group A and B samples which produced using relatively low pressure. Even though sintering occurred between nano silver particles; there was no significant diffusion between silver coated substrates or silver coated dummy chips and nano silver particles as revealed by the fracture surface examination. Additionally, the presence of large voids in the fracture surface was the indication of insufficient sintering. Since the strength values in two groups were similar the effect of ultrasonic pressure could not be determined as the flip chip bonder machine was not capable of applying higher pressures. In this case, the ultrasonic force effect on bonding strength is not clear. On the other hand, the strength values were quite promising as the type and magnitude of the sintering pressure changes. The results were quite high when compared with just the ultrasonic force test condition as pressure increased to 5 MPa. The strength values increased by 2, 4 and 8 times for Group C, D and E samples, respectively, due to increased neck area. However, each group's strength values were different due to different degrees of sintering.

Group C joints performed in vacuum exhibited strengths around ~9 MPa which was actually half of the strength of Group D joints (~17 MPa). The reason for relatively lower strength in Group C was attributed to insufficient burning out of organics in the vacuum environment. On the other hand, the average bonding strength was found to be 32.3 MPa for the group which was even higher than that of the Group D sample. Although the test parameters were the same for both Group D and E samples processed in air, the application of pressure was different. The pneumatic press test fixture supplied the constant pressure over the entire processing in Group E samples; however, the pressure (applied by screws) gradually decreased and its effect was lost in Group D samples. During the sintering process, the layer thickness of nano silver

paste decreased due to disappearance of organic materials and engaging nano particles due to persistent pressure. The average shear strengths are presented in Figure 4.9

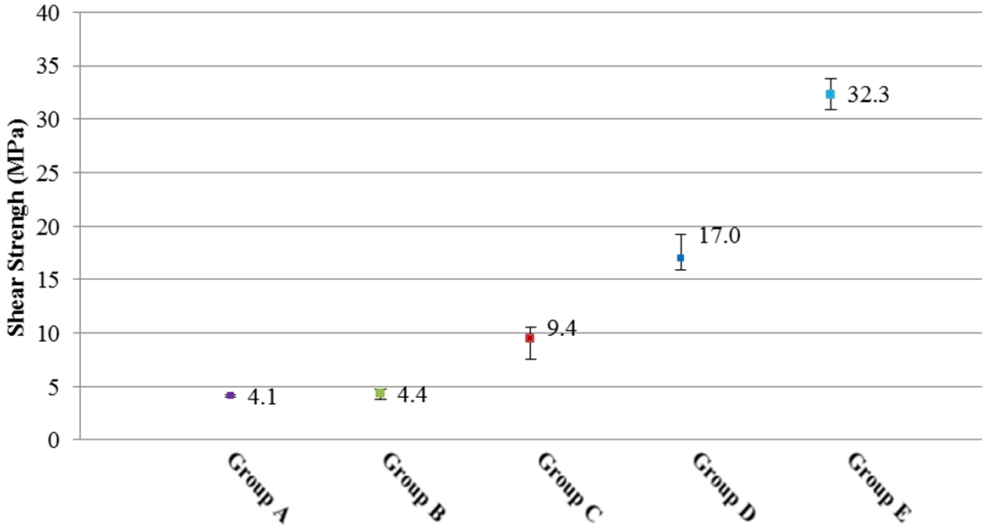


Figure 4.9 The average shear strength of the joints processed in different conditions

The comparison of the literature and the present study results are represented in Figure 4.10. The red square shape label shows current study results. At 5 MPa assisted pressure, the shear strength has been scattered between 30 MPa to 41 MPa in the literature depending on test conditions. It is difficult to evaluate this comparison because there are several parameters which affect the bonding quality. The closest test condition is the Gang Chen and et al. [51] study, which is marked by a red circle in the figure. They reported 39.1 MPa shear strength at 275 °C and 5 MPa assisted pressure for 10 minutes.

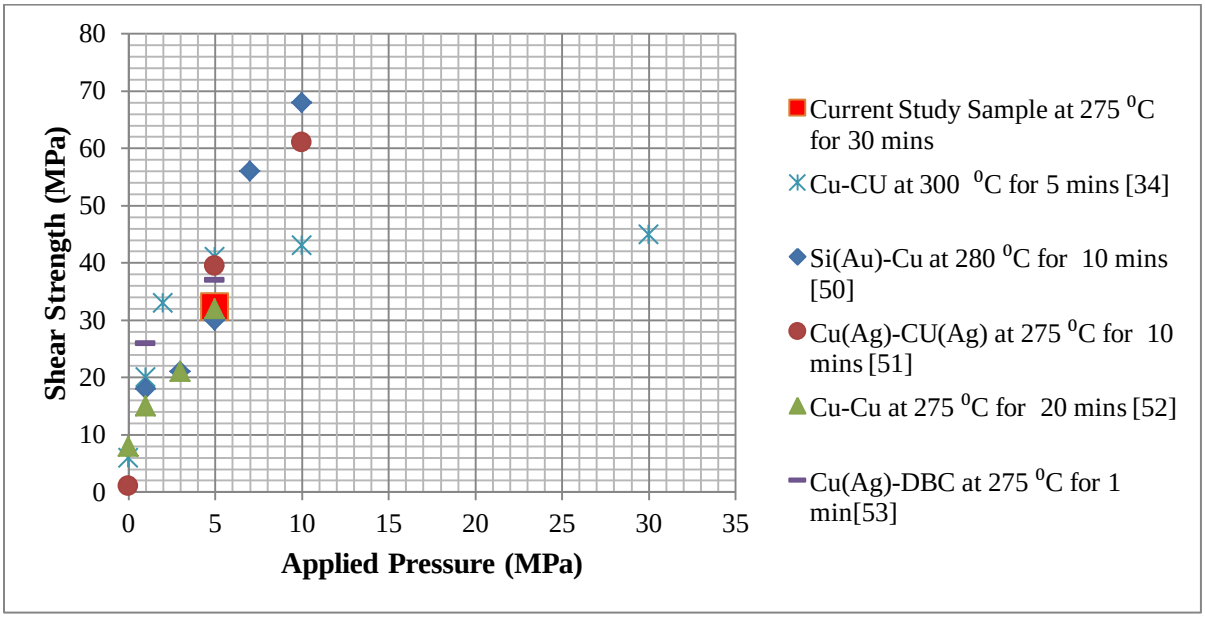


Figure 4.10 Comparison with the shear strengths dependent on pressure effect.

## 4.3 Electrical Properties

Electrical resistance means that the flow of current through a material faces resistance. Resistance depends on the chemical composition of materials, sample length, and cross-sectional area. The electrical resistivity and conductivity are material properties and their relationship is inversely proportional to each other. The sheet resistance is a thin film resistance over nominal uniform thickness. In this study, electrical resistivity was calculated for each test condition. Figure 4.11 shows the average electrical resistivity of the sintered nano silver layers, which were produced using various manufacturing processes.

The completed sintering event and densification of the sintering region mainly impact the electrical properties of the sintered nano silver layer [71]. Group A, B, and C had very high resistivity, 125.5, 109.3, and 119.1 μΩ.cm, respectively. Group D had relatedly lower resistivity, 17.9 μΩ.cm. The closest resistivity of the bulk silver (1.55 μΩ.cm) one was obtained in group E, 7.8 μΩ.cm. This significantly better performance is due mainly to the average neck size being the largest and complete burning out of organic materials, which keep separating the conductive nano particles. The results indicated that the resistivity was reduced and became closer to bulk silver resistivity value when nano particles engaged each other well in a continuous and conductive path.

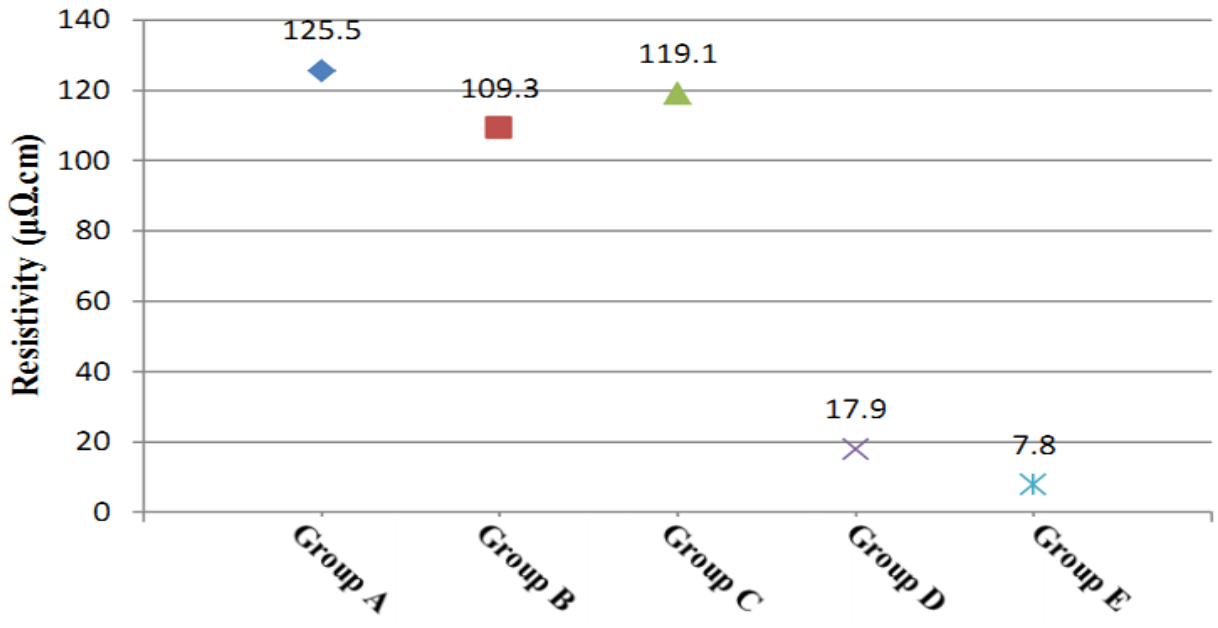


Figure 4.11 Electrical resistivity for each test group

Microstructural study reveals the relationship between sintered nano silver layer resistivity and neck growing. The main reason of reduction of resistivity is physical contact between particles. The microstructural differences between groups are presented in Figure 4.3 . The resistivity aspect of these microstructures is that nano silver particles were well-bonded to each other. Densifications of microstructures increase while resistivity of layers decreases. Grain size, porosity of structure and resistivity relationship have been defined as mathematical models in the literature [77], [78]. A large grain size and less porous structure have lower resistivity than small grain size and a more porous one. Assisted pressure created less porous structures and a well sintered region.

Group A and B have very similar microstructure; consequently, their resistivity measurements confirmed this microstructural similarity. The sintering atmosphere was air, and organic materials were burnt out completely. However, the growing necks between particles were limited due to lack of sintering pressure. Less physical contact between particles is implied; thus, the resistivity of these samples is higher. Lack of oxygen atmosphere prevented the burning out of organic materials completely in vacuum. Less physical contact and higher resistivity for group C is indicated. Even though tests were held in air for group D and E, it is also apparent that the absolute resistivity is higher for group D compared with

constant pressure test conditions for group E due to improvement of nano particle connections with constant pressure.

Based on the comparison of the measured results to the bulk resistivity of silver, a conclusion can be drawn that group E had a conductive path because of a well-sintered region and approached bulk silver resistivity. The results show that the resistivity reduced with densification of sintered layer and well-sintered region which means more physical contact. The same result has been concluded regarding the microstructural examination.

Figure 4.12 represents comparison of electrical resistivity between common used solders and Group E. The resistivity decreases using nano silver paste, however, sintered silver layer resistivity is still high according to bulk silver resistivity.

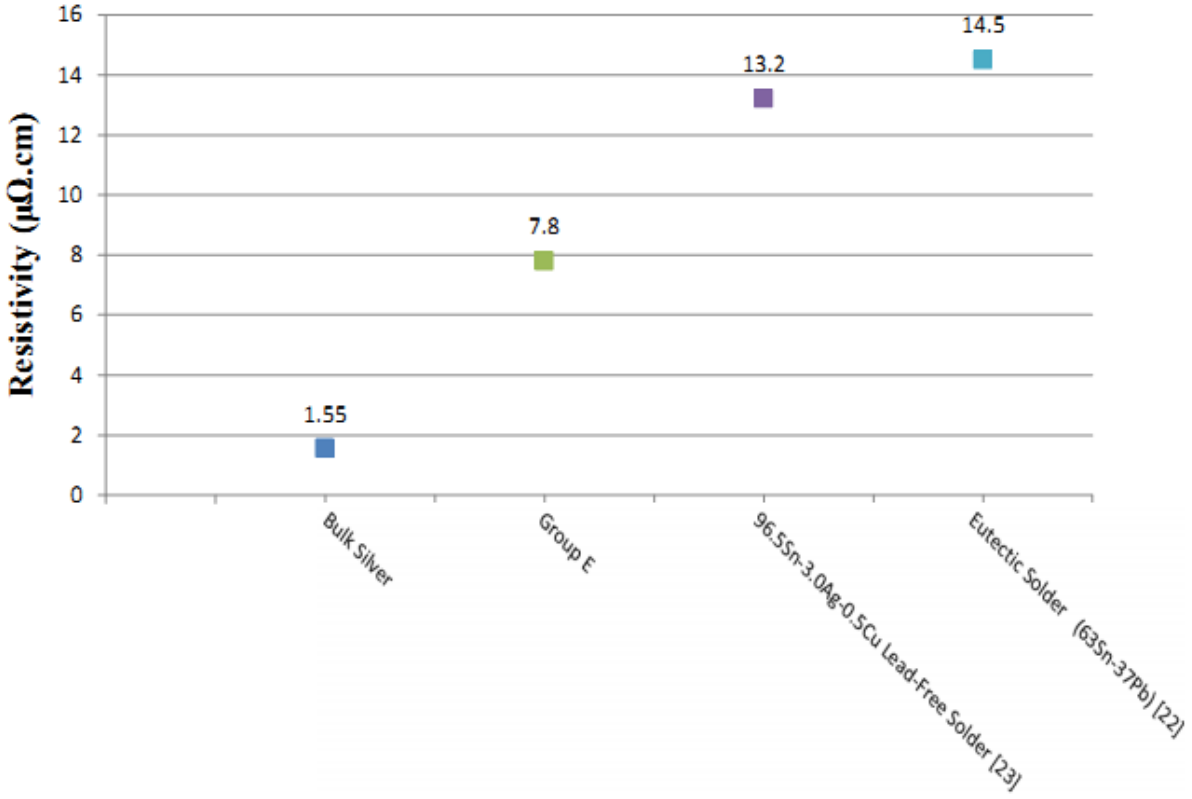


Figure 4.12 Comparison of electrical resistivity between sintered nano silver layer (Group E), commonly used solders and bulk silver.

# Chapter 5
# Conclusions and Outlook

## 5.1 Conclusion

In this thesis, die attach material was studied for power modules in automotive applications. The die attach material is one of the most common reliability issues for packaging. Nano silver paste was chosen as a die attach material and different fabrication methods were applied to bond chips and substrate to each other. Silver coated substrate and dummy chips were successfully bonded to each other using nano silver paste.

Ultrasonic force effect on bonding was investigated. A weak bonding was obtained due to lack of assisted pressure.

Sintering atmosphere effect was studied. The joining process was carried out in air and vacuum. The result reveals that air atmosphere clearly gives better bonding between the dummy chip and substrate in comparison with vacuum atmosphere due to lack of oxygen.

Two different tests were carried out in air atmosphere. The only difference was the assisted pressure condition. This test concluded that assisted pressure has a strong impact on bonding quality. The constant pressure produced stronger bonding strength and less resistivity of the sintered nano silver layer than a gradually declining pressure.

According to microstructural examination, mechanical and electrical characterizations, the conclusion can be drawn that sintering pressure and test atmosphere strongly influence the bonding quality. The sintering pressure helps to improve mechanical and electrical properties of nano silver paste not only because of an increase in contact surface for sintering, but also an improvement in outgassing of organic materials. Additionally, oxygen is needed to burn out organic materials. Air atmosphere aids the sintering event due to elimination of organic materials.

## 5.2 Future Work

In this study, the processing parameters, which are sintering temperature, sintering time, and assisted pressure, were kept constant. It might be useful to study the effects of these parameters on bonding for each test condition. While one parameter is changed such as temperature, the rest of the parameters are kept the same. This test might reveal which parameter is vital for bonding quality.

The ultrasonic force effect was studied. However, sintering pressure was 0.01 MPa and it was not enough to reveal the ultrasonic force impact on bonding due to lack of equipment. Further investigation is needed.

Additionally, the reliability tests can be applied for each test condition. For microelectronic reliability, thermal cycling and power cycling tests are commonly used to reveal reliability of a given device under certain conditions. The most common standard tests are Jesd22-A104E and Jesd22-A122, which are published by JEDEC solid state technology association. These test conditions can be applied. After certain cycling, microstructural examination might give a better understanding of the nano silver joining reliability under our test conditions.

# Appendix A

## Parameters of Some Studies

Appendix A gives a summary of studies carried out at various processing conditions using different silver based pastes and elementary Silver powders. Commonly studied variables are the types of die attach materials and their sizes, coating of substrates and chips, sintering temperature, pressure and time, heating rate, test methods, and the shear strength of joining.

| Application | Die attach material, thickness and size | Test methods | Electroplating material substrate | Electroplating thickness substrate | Electroplating material chip | Electroplating thickness chip | Sintering time | Sintering pressure (MPa) | Sintering temperature | Heating rate | The shear strength (ultimate shear stress) (MPa) | References |
|---|---|---|---|---|---|---|---|---|---|---|---|---|
| Power electronic | Nano silver, 75 micron before drying, >50nm | Power cycling | DBC, Ag | 5 microns | Si, Ag | 5 microns | 60 second | 5 | 275 | 600 K/min | 40.1 | [79] |

| | | | | | | | | | | | | |
|---|---|---|---|---|---|---|---|---|---|---|---|---|
| LED | Nano silver, 50 micron before drying and 15 micron after, - (>50nm) | Clamp of micro tension-torsional fatigue | Lead frame, Ag/Ni | - | Si, Au back coating | - | 20 mins | - | 275 | - | 28.7 | [19] |
| Power electronic | Nano silver, 50 micron, (>50nm) | Single lap shear joint, fatigue | Cu,- | - | Cu,- | - | 30 mins | - | 280 | - | (28 ) | [58] |
| Power electronic | Nano silver, before 60-80 micron after 30-40 micro, - (50nm) | Power cycling | DBA, Ni flash Au/Ag | - | AlSiCu/ Cr/ Ni/Ag | - | 60 second | 5 | 275 | - | - | [80] |
| | | | DBC, Ni flash Au | - | AlSiCu | - | 60 second | 5 | 275 | - | - | |
| | | | DBC, Ni flash Au/Ag | - | AlSiCu/ Cr/ Ni/Ag | - | 60 second | 5 | 275 | - | - | |
| | | | DBA, Ni flash Au | - | AlSiCu/ Cr/ Ni/Ag | - | 60 second | 5 | 275 | - | - | |

| | | | | | | | | | | | | | |
|---|---|---|---|---|---|---|---|---|---|---|---|---|---|
| Power electronic | Nano silver before 90 after 50 micro, 30 nm | Fabrication and mechanical test | Cu, Ag | 10 microns | Cu, Ag | 10 microns | 600 - 10 seconds | 5 - 1 | 225 - 275 | - | 30 | 55 | [81] |
| Microelectronic packing | Nano silver 50 micron, >50 nm | Lab shear joint test mechanism | Cu, - | - | Cu, - | - | 30 mins | - | 280 | - | 28 (at room temp.), 13.3 (325) | | [59] |
| Power electronic | Nano silver, 50 + 10 micron, >50nmm | Fabrication and electrical testing | DBC, - | - | Al, Ag | - | 3 mins | 1 to 12 | 275 | - | 25 | 77 | [82] |

| | | | | | | | | | | | | | |
|---|---|---|---|---|---|---|---|---|---|---|---|---|---|
| Electronic packing | Nano silver, 45 micron, 20 nm (they produced) | Fabrication and mechanical test | Cu, Ni and Ag | Ni 2 microns, 5 microns Ag | Cu, Ni and Ag | Ni 2 microns, 5 microns Ag | 20 mins | - | 150<br>200 | 5 K/min | 17 +- 5<br>25 +- 5 | | [83] |
| Flexible electronic | Nano silver , - , 40 nm | Fabrication and mechanical test | Cu, Ag | - | Cu, Ag | - | 30 mins | 0-5 | 250 | 20 C/min | 15 | 50 | [35] |
| Power electronic | Nano silver, before 50 +10 micron after 20 micron, ( > 50nm) | Fabrication and mechanical test | DBC, Ag | a few hundred nanometers | Al, Ag | a few hundred nanometers | 10-30 mins | 0-3 | 275 | preheated | 11 | 53.8 | [84] |

| | | | | | | | | | | | | | | |
|---|---|---|---|---|---|---|---|---|---|---|---|---|---|---|
| Microelectronic packing | Nano silver , - ,70 nm | Fabrication and mechanical test | PCB, ENIG (Electroless Ni Immersed Gold) coated Cu pads | - | Si,- | - | 30-60-90 mins | 1-5-10 | 170-200-230 | - | 0.2 | 0.8 | [85] | |
| Power electronic | Ag flake + nano silver, before 200 microns, - | Fabrication and mechanical test | Cu, Ti and Ag | Ti 40 nanometers, Ag 2 microns | Cu, Ti and Ag | Ti 40 nanometers, Ag 2 microns | 30 mins | 0.4 | 250 | - | 15 | | [61] | |
| Power modules | Nano silver, before 50 and 100 micron after 25 and 55 micron, 20 nm | Fabrication, mechanical test and thermal cycling | DBC; Ag, Au or Cu | - | Si | - | 45 secs - 5 mins | 5-10 | 230 -250 | - | Cu | Au | Ag | [86] |
| | | | | | | | | | | | 20 | >25 | >25 | |

| | | | | | | | | | | | | | | |
|---|---|---|---|---|---|---|---|---|---|---|---|---|---|---|
| Power modules | Nano silver, before 100 micron, -(20nm) | Fabrication, mechanical test and thermal cycling | DBC; Au, Ag, and Cu | - | Si | - | - | ~ 10 | < 300 | - | Cu<br>36 | Ni/Au<br>35 | Ag<br>36 | [87] |
| Microelectronic packing | Nano Ag +Cu, 50 micron, Ag-40 nm and Cu-50 nm | Fabrication, mechanical test and thermal aging | Cu; Cu, Ag, Au | 0.5 microns | Cu; Cu, Ag, Au | 0.5 microns | 30 mins | - | 380 | 5 C/min | Ag<br>52.6 | Cu<br>42 | Au<br>34.4 | [41] |

# Appendix B

# Datasheet

Nano silver paste datasheet was received from Nihon Superior CO., LTD.

# ALCONANO® ANP-1

## Nano-Silver Bonding Paste

**Alconano** bonding pastes, based on unique nano-silver particles passivated with alcohol derivatives[1], can be used in a wide variety of applications where a reliable lead-free connection with high electrical and thermal conductivity is required.

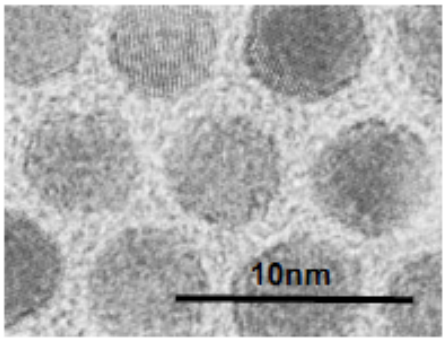


Alcohol passivated silver nano particles

The highly active surface of the nano-silver particles makes it possible to sinter at relatively low temperatures to produce a bond that can operate at temperatures greater than 600°C.

Since the carrier solvent as well as the passivating molecules contain only carbon, hydrogen and oxygen they leave no residues that could contribute to the deterioration of the joint in service.

Applications for Alconano pastes include

- Die attach for power semiconductors where the high operating temperature provides an advantage over high-lead solders and conductive adhesives
- Package on Package (PoP)
- High I/O density component attach

# References


[1] "Inventory of U.S. Greenhouse Gas Emissions and Sinks: 1990 - 2013," U.S. Environmental Protection Agency, Washington, EPA 430-R-15-004, 2015.

[2] "DieselNet: Diesel Exhaust Emission Standards." [Online]. Available: http://www.dieselnet.com/standards/#eu; [Accessed: 05-Dec-2015].

[3] L. Skogström, "A Novel Approach for Rapid Reliability Assessment of Power Electronics under Combined Vibration and Thermal Loading," MASc Thesis, School of Electrical Engineering, Aalto University, 2014.

[4] C. C. Chan, "The state of the art of electric, hybrid, and fuel cell vehicles," *Proc. IEEE*, vol. 95, no. 4, pp. 704–718, 2007.

[5] Z. Q. Zhu and D. Howe, "Electrical Machines and Drives for Electric, Hybrid, and Fuel Cell Vehicles," *Proc. IEEE*, vol. 95, no. 4, pp. 746–765, 2007.

[6] J. L. Fock-Sui-Too, B. Chauchat, P. Austin, P. Tounsi, M. Mermet-Guyennet, and R. Meuret, "Performance and reliability testing of modern IGBT devices under typical operating conditions of aeronautic applications," *Microelectron. Reliab.*, vol. 48, no. 8–9, pp. 1453–1458, 2008.

[7] D. W. Hart, *Power Electronics*. Tata McGraw-Hill Education, 2011.

[8] S. West, "IGBT Applications Handbook," HBD871/D, On Semiconductor, Denver, Colorado, 2014.

[9] R. W. Johnson, J. L. Evans, P. Jacobsen, J. R. Thompson, and M. Christopher, "The changing automotive environment: High-temperature electronics," *IEEE Trans. Electron. Packag. Manuf.*, vol. 27, no. 3, pp. 164–176, 2004.

[10] T. Stockmeier, "From Packaging to 'Un'-Packaging - Trends in Power Semiconductor Modules," pp. 12–19, 2008.

[11] S. Zhou, L. Zhou, S. Liu, P. Sun, Q. Luo, and J. Wu, "The Application of Approximate Entropy Theory in Defects Detecting of IGBT Module," *Act. Passiv. Electron. Components*, vol. 2012, pp. 1–7, 2012.

[12] U. Scheuermann, "Reliability of Planar SKiN Interconnect Technology," in *7th International Conference on Integrated Power Electronics Systems (CIPS)*, 2012, pp. 464–471.

[13] J. G. Bai, J. Yin, Z. Zhang, G. Q. Lu, and J. D. van Wyk, "High-temperature operation of SiC power devices by low-temperature sintered silver die-attachment," *IEEE Trans. Adv. Packag.*, vol. 30, no. 3, pp. 506–510, 2007.

[14] H. S. Chin, K. Y. Cheong, and A. B. Ismail, "A Review on Die Attach Materials for SiC-Based High-Temperature Power Devices," *Metall. Mater. Trans. B*, vol. 41, no. 4, pp. 824–832, 2010.

[15] Z. Liang, "Status and trend of automotive power packaging," in *Proceedings of the International Symposium on Power Semiconductor Devices and ICs*, 2012, pp. 325–331.

[16] P. Dietrich, "Trends in automotive power semiconductor packaging," *Microelectron. Reliab.*, vol. 53, no. 9–11, pp. 1681–1686, 2013.

[17] A. M. Bento, K. D. Roth, and Y. Zuo, "Vehicle Lifetime Trends and Scrappage Behavior in the U.S. Used Car Market," *Available SSRN 2262593*, no. 607, pp. 592–626, 2013.

[18] A. Wintrich, U. Nicolai, W. Tursky, and T. Reimann, *Application Manual Power Semiconductors*. SEMIKRON International GmbH, Nuremberg, Germany, 2011.

[19] X. Li, X. Chen, D. Yu, and G. Lu, "Study on adhesive reliability of low-temperature sintered high power LED modules," in *2010 11th International Conference on Electronic Packaging Technology & High Density Packaging*, 2010, pp. 1371–1376.

[20] G.-Q. L. G.-Q. Lu, J. N. Calata, Z. Z. Z. Zhang, and J. G. Bai, "A lead-free, low-temperature sintering die-attach technique for high-performance and high-temperature packaging," in *Proceedings of the Sixth IEEE CPMT Conference on High Density Microsystem Design and Packaging and Component Failure Analysis (HDP '04)*, 2004, pp. 42–46.

[21] "EUR-Lex - 32002L0095 - EN - EUR-Lex." [Online]. Available: http://eur-lex.europa.eu/legal-content/EN/TXT/?uri=CELEX:32002L0095. [Accessed: 03-Jan-2016].

[22] "Eutectic Solder (63Sn-37Pb) - ASTM B 32 Grade Sn63." [Online]. Available: http://www.matweb.com/search/DataSheet.aspx?MatGUID=3a5c8bc670914d588b26ab0b994d88cb. [Accessed: 13-Jan-2016].

[23] T. Sawamura and T. Igarashi, "Difference Between Various Sn / Ag / Cu Solder Compositions," Almit LTD, 2005.

[24] K. Suganuma, S. J. Kim, and K. S. Kim, "High-temperature lead-free solders: Properties and possibilities," *JOM J. Miner. Met. Mater. Soc.*, vol. 61, no. 1, pp. 64–71, 2009.

[25] J. G. Bai, Z. Z. Zhang, J. N. Calata, and G. Q. Lu, "Low-temperature sintered nanoscale silver as a novel semiconductor device-metallized substrate interconnect material," *IEEE Trans. Components Packag. Technol.*, vol. 29, no. 3, pp. 589–593, 2006.

[26] D. S. Eddy and D. R. Sparks, "Application of MEMS technology in automotive sensors and actuators," in *Proceedings of the IEEE*, 1998, pp. 1747–1755.

[27] J. Watson and G. Castro, "A review of high-temperature electronics technology and applications," *J. Mater. Sci. Mater. Electron.*, vol. 26, no. 12, pp. 9226–9235, 2015.

[28] H. Zhang, S. S. Ang, H. a. Mantooth, and S. Krishnamurthy, "A high temperature, double-sided cooling SiC power electronics module," in *2013 IEEE Energy Conversion Congress and Exposition*, 2013, pp. 2877–2883.

[29] J. Steger, A. Chip, and C. Substrate, "A New Generation of Power Modules with Sinter-Technology for the Automotive Industry .," pp. 60–62, 2011.

[30] G. Chen, D. Han, Y.-H. Mei, X. Cao, T. Wang, X. Chen, and G.-Q. Lu, "Transient Thermal Performance of IGBT Power Modules Attached by Low-Temperature Sintered Nanosilver," *Device Mater. Reliab. IEEE Trans.*, vol. 12, no. 1, pp. 124–132, 2012.

[31] L. Meysenc, M. Jylhäkallio, and P. Barbosa, "Power electronics cooling effectiveness versus thermal inertia," *IEEE Trans. Power Electron.*, vol. 20, no. 3, pp. 687–693, 2005.

[32] H. A. Alarifi, "Ag Nanoparticles and their Application in Low-Temperature Bonding of Cu," PhD Dissertations, Mechanical Engineering Dept., University of Waterloo, Canada, 2013.

[33] J. Bai and G. Lu, "Thermomechanical Reliability of Low-Temperature Sintered Silver Die Attached SiC Power Device Assembly," *IEEE Trans. Device Mater. Reliab.*, vol. 6, no. 3, pp. 436–441, 2006.

[34] E. Ide, S. Angata, A. Hirose, and K. F. Kobayashi, "Metal-metal bonding process using Ag metallo-organic nanoparticles," *Acta Mater.*, vol. 53, no. 8, pp. 2385–2393, 2005.

[35] J. Yan, G. Zou, A. P. Wu, J. Ren, J. Yan, A. Hu, and Y. Zhou, "Pressureless bonding process using Ag nanoparticle paste for flexible electronics packaging," *Scr. Mater.*, vol. 66, no. 8, pp. 582–585, 2012.

[36] B. W. C. Butterman and H. E. Hilliard, "Silver," U.S. Geological Survey, Reston, Virginia,Open-File Report 2004-1251, 2005.

[37] H. Schwarzbauer and R. Kuhnert, “Novel large Area Joining Technique for Improved Power Device Performance,” in *Industry Applications Society Annual Meeting, 1989., Conference Record of the 1989 IEEE*, 1989, pp. 1348–1351.

[38] J. Kähler, N. Heuck, A. Wagner, A. Stranz, E. Peiner, and A. Waag, “Sintering of copper particles for die attach,” *IEEE Trans. Components, Packag. Manuf. Technol.*, vol. 2, no. 10, pp. 1587–1591, 2012.

[39] T. Bakhishev and V. Subramanian, “Investigation of Gold Nanoparticle Inks for Low-Temperature Lead-Free Packaging Technology,” *J. Electron. Mater.*, vol. 38, no. 12, pp. 2720–2725, 2009.

[40] V. R. Manikam, K. A. Razak, and K. Y. Cheong, “Reliability of sintered Ag80-Al20 die attach nanopaste for high temperature applications on SiC power devices,” *Microelectron. Reliab.*, vol. 53, no. 3, pp. 473–480, 2013.

[41] K. S. Tan and K. Y. Cheong, “Mechanical properties of sintered Ag–Cu die-attach nanopaste for application on SiC device,” *Mater. Des.*, vol. 64, pp. 166–176, 2014.

[42] Z. Esen, “Production and Characterization of Porous Titanium Alloys,” PhD Dissertations, Metallurgical and Materials Engineering Department, Middle East Technical, 2007.

[43] R. M. German, *Liquid Phase Sintering*. Boston, MA: Springer US, 1985.

[44] R. M. German, *Sintering Theory and Practice*. Solar-Terrestrial Physics (Solnechno-zemnaya fizika), 1996.

[45] P. Peng, “Metallurgical Issues in Low-Temperature Joining of Silver Nanowires,” PhD Dissertations, Mechanical Engineering - Nanotechnology Dept., University of Waterloo, Canada, 2014.

[46] M. Zhou, Z. Wei, H. Qiao, L. Zhu, H. Yang, and T. Xia, “Particle Size and Pore Structure Characterization of Silver Nanoparticles Prepared by Confined Arc Plasma,” *J. Nanomater.*, vol. 2009, pp. 1–5, 2009.

[47] A. Hu, J. Y. Guo, H. Alarifi, G. Patane, Y. Zhou, G. Compagnini, and C. X. Xu, “Low temperature sintering of Ag nanoparticles for flexible electronics packaging,” *Appl. Phys. Lett.*, vol. 97, no. 15, p. 153117, 2010.

[48] K. S. Siow, “Are Sintered Silver Joints Ready for Use as Interconnect Material in Microelectronic Packaging?,” *J. Electron. Mater.*, vol. 43, no. 4, pp. 947–961, 2014.

[49] R. Khazaka, L. Mendizabal, and D. Henry, “Review on Joint Shear Strength of Nano-Silver Paste and Its Long-Term High Temperature Reliability,” *J. Electron. Mater.*, vol. 43, no. 7, pp. 2459–2466, 2014.

[50] L. a. Navarro, X. Perpiña, M. Vellvehi, and X. Jordà, “Silver nano-particles sintering process for the die-attach of power devices for high temperature applications,” *Ing. Mecãnica Tecnol. y Desarro.*, vol. 4, no. 3, pp. 97–102, 2012.

[51] C. Attachment, G. Chen, Y. Cao, Y. Mei, D. Han, G. Lu, and X. Chen, “Pressure-Assisted Low-Temperature Sintering of Nanosilver Paste for 5x5 mm2 -Chip Attachment,” *IEEE Trans. Components, Packag. Manuf. Technol.*, vol. 2, no. 11, pp. 1759–1767, 2012.

[52] T. G. Lei, J. N. Calata, G. Lu, X. Chen, and S. Luo, “Low-temperature sintering of nanoscale silver paste for attaching large-area (>100 mm2) chips,” *IEEE Trans. COMPONENTS Packag. Technol.*, vol. 33, no. 1, pp. 98–104, 2010.

[53] M. Knoerr and A. Schletz, “Power semiconductor joining through sintering of silver nanoparticles: Evaluation of influence of parameters time, temperature and pressure on density, strength and reliability,” in *Proc. 6th International Conference on Integrated Power Electronics Systems (CIPS)*, 2010, p. 10.3.

[54] T. Wang, X. Chen, G.-Q. Lu, and G.-Y. Lei, “Low-Temperature Sintering with Nano-Silver Paste in Die-Attached Interconnection,” *J. Electron. Mater.*, vol. 36, no. 10, pp. 1333–1340, 2007.

[55] G. Zou, J. Yan, F. Mu, A. Wu, J. Ren, A. Hu, and Y. N. Zhou, “Low Temperature Bonding of Cu Metal through Sintering of Ag Nanoparticles for High Temperature Electronic Application,” *Open Surf. Sci. J.*, vol. 3, pp. 70–75, 2011.

[56] Y. Morisada, T. Nagaoka, M. Fukusumi, Y. Kashiwagi, M. Yamamoto, and M. Nakamoto, “A low-temperature bonding process using mixed Cu-Ag nanoparticles,” *J. Electron. Mater.*, vol. 39, no. 8, pp. 1283–1288, 2010.

[57] K. S. Siow, “Mechanical properties of nano-silver joints as die attach materials,” *J. Alloys Compd.*, vol. 514, pp. 6–19, 2012.

[58] X. Lil, X. Chen, and G. Lu, “Isothermal Low Cycle Fatigue Behavior of Nano-Silver Sintered Single Lap Shear Joint,” in *2012 International Conference on Electronic Packaging Technology & High Density Packaging*, 2012, pp. 1209–1215.

[59] Y. Tan, X. Li, and X. Chen, “Fatigue and dwell-fatigue behavior of nano-silver sintered lap-shear joint at elevated temperature,” *Microelectron. Reliab.*, vol. 54, no. 3, pp. 648–653, 2014.

[60] E. A. Holm, J. D. Puskar, M. Reece, V. Tikare, C. Garcia, and L. N. Brewer, “Nanocrystal-enabled Solid State Bonding,” Report SAND2010-7013, Sandia National Laboratories,Livermore, California, 2010.

[61] H. Zhang, S. Nagao, S. Park, S. Koga, T. Sugahara, and K. Suganuma, “Nano-SiC added Ag paste sintering die-attach for SiC power devices,” in *ELECTRONICS SYSTEM-INTEGRATION CONFERENCE (ESTC)*, 2014, pp. 1–4.

[62] H. Ogura, M. Maruyama, R. Matsubayashi, T. Ogawa, S. Nakamura, T. Komatsu, H. Nagasawa, A. Ichimura, and S. Isoda, “Carboxylate-passivated silver nanoparticles and their application to sintered interconnection: A replacement for high temperature lead-rich solders,” *J. Electron. Mater.*, vol. 39, no. 8, pp. 1233–1240, 2010.

[63] Y. Mei, Y. Cao, G. Chen, X. Li, G. Q. Lu, and X. Chen, “Rapid sintering nanosilver joint by pulse current for power electronics packaging,” *IEEE Trans. Device Mater. Reliab.*, vol. 13, no. 1, pp. 258–265, 2013.

[64] Yu Seong Lee, Changhun Yun, Ki Hyun Kim, Wan Ho Kim, Sie-Wook Jeon, June Key Lee, and Jae Pil Kim, “Laser-Sintered Silver Nanoparticles as a Die Adhesive Layer for High-Power Light-Emitting Diodes,” *IEEE Trans. Components, Packag. Manuf. Technol.*, vol. 4, no. 7, pp. 1119–1124, 2014.

[65] S. Magdassi, M. Grouchko, O. Berezin, and A. Kamyshny, “Triggering the sintering of silver nanoparticles at room temperature,” *ACS Nano*, vol. 4, no. 4, pp. 1943–1948, 2010.

[66] “Oxygen-free Electronic Copper (OFE), UNS C10100, H04 Temper, plate (25 mm Thick).” [Online]. Available: http://www.matweb.com/search/DataSheet.aspx?MatGUID=97e1284ad77b40f4a0513933519f49dd. [Accessed: 17-Jan-2016].

[67] S. Fu, Y. Mei, G.-Q. Lu, X. Li, G. Chen, and X. Chen, “Pressureless sintering of nanosilver paste at low temperature to join large area (≥100mm2) power chips for electronic packaging,” *Mater. Lett.*, vol. 128, pp. 42–45, 2014.

[68] “Quartz (SiO 2 ).” [Online]. Available:

http://www.matweb.com/search/datasheet.aspx?MatGUID=8715a9d3d1a149babe853b465c79f73e. [Accessed: 18-Jan-2016].

[69] D. Page, L. Burrows, C. Kowalski, and J. Valencia, "Dektak 8 Advanced Development Profiler Manual," Veeco Instruments Inc.,Tucson, Arizona, 2004.

[70] S. Merilampi, T. Laine-Ma, and P. Ruuskanen, "The characterization of electrically conductive silver ink patterns on flexible substrates," *Microelectron. Reliab.*, vol. 49, no. 7, pp. 782–790, 2009.

[71] J. R. Greer and R. A. Street, "Thermal cure effects on electrical performance of nanoparticle silver inks," *Acta Mater.*, vol. 55, no. 18, pp. 6345–6349, 2007.

[72] X. Li, G. Chen, X. Chen, G.-Q. Lu, L. Wang, and Y.-H. Mei, "Mechanical property evaluation of nano-silver paste sintered joint using lap-shear test," *Solder. Surf. Mt. Technol.*, vol. 24, no. 2, pp. 120–126, 2012.

[73] A. Hattiangadi and A. Bandyopadhyay, "Strength Degradation of Nonrandom Porous Ceramic Structures under Uniaxial Compressive Loading," *J. Am. Ceram. Soc.*, vol. 83, no. 11, pp. 2730–2736, 2000.

[74] R. W. Rice, "Comparison of physical property-porosity behaviour with minimum solid area models," *J. Mater. Sci.*, vol. 31, pp. 1509–1528, 1996.

[75] R. W. Rice, "Evaluation and extension of physical property-porosity models based on minimum solid area," *J. Mater. Sci.*, vol. 31, no. 1, pp. 102–118, 1996.

[76] R. W. Rice, "Evaluating Porosity Parameters for Porosity-Property Relations," *J. Am. Ceram. Soc.*, vol. 76, no. 7, pp. 1801–1808, 1993.

[77] D. A. Roberson, R. B. Wicker, L. E. Murr, K. Church, and E. MacDonald, "Microstructural and process characterization of conductive traces printed from Ag particulate inks," *Materials (Basel).*, vol. 4, no. 6, pp. 963–979, 2011.

[78] C. Huang, M. F. Becker, J. W. Keto, and D. Kovar, "Annealing of nanostructured silver films produced by supersonic deposition of nanoparticles," *J. Appl. Phys.*, vol. 102, no. 5, 2007.

[79] M. Knoerr, S. Kraft, and A. Schletz, "Reliability assessment of sintered nano-silver die attachment for power semiconductors," in *Proc. 12th Electronics Packaging Technology Conference (EPTC)*, 2010, pp. 56–61.

[80] S. Kraft, A. Schletz, and M. März, "Reliability of Silver Sintering on DBC and DBA Substrates for Power Electronic Applications," in *Integrated Power Electronics Systems (CIPS), 7th International Conference*, 2012, pp. 1–6.

[81] Y. Mei, G. Chen, Y. Cao, X. Li, D. Han, and X. Chen, "Simplification of Low-Temperature Sintering Nanosilver for Power Electronics Packaging," *J. Electron. Mater.*, vol. 42, no. 6, pp. 1209–1218, 2013.

[82] H. Zheng, D. Berry, J. N. Calata, K. D. T. Ngo, S. Member, S. Luo, and G. Lu, "Low-Pressure Joining of Large-Area Devices on Copper Using Nanosilver Paste," *IEEE Trans. COMPONENTS Packag. Technol.*, vol. 3, no. 6, pp. 915–922, 2013.

[83] S. Wang, H. Ji, M. Li, J. Kim, H. Kim, and S. Korea, "Fabrication of interconnects using pressureless low temperature sintered Ag nanoparticles," *Mater. Lett. J.*, vol. 85, pp. 61–63, 2012.

[84] K. Xiao, J. N. Calata, H. Zheng, K. D. T. Ngo, and G. Q. Lu, "Simplification of the nanosilver sintering process for large-area semiconductor chip bonding: Reduction of hot-pressing temperature below 200 °c," *IEEE Trans. Components, Packag. Manuf. Technol.*, vol. 3, no. 8, pp. 1271–1278, 2013.

[85] T. Fałat, K. Stojek, P. Matkowski, B. Płatek, J. Felba, and A. Mościcki, "Influence of Sintering Process Parameters on Mechanical Strength of Joints Based on Silver Nano Particles," in *16th Electronics Packaging Technology Conference (EPTC)*, 2014, pp. 801–804.

[86] X. Zhao, Yimin; Wu, Yibo; Evans, Kim; Swingler, John; Jones, Steve; Dai, "Evaluation of Ag sintering die attach for high temperature power module applications," in *15th International Conference on Electronic Packaging Technology*, 2014, pp. 200–204.

[87] F. Le Henaff, S. Azzopardi, J. Y. Deletage, E. Woirgard, S. Bontemps, and J. Joguet, "A preliminary study on the thermal and mechanical performances of sintered nano-scale silver die-attach technology depending on the substrate metallization," *Microelectron. Reliab.*, vol. 52, no. 9–10, pp. 2321–2325, 2012.